TAMPERE UNIVERSITY OF TECHNOLOGY

ALAAEDDIN Y. M. LOULOU

ENHANCED OFDM FOR FRAGMENTED SPECTRUM USE

Master of Science Thesis

Examiners: Prof. Markku Renfors and
Dr. Juha Yli-Kaakinen
Examiner and topic approved by the
Faculty Council of the Faculty of
Computing and Electrical Engineering
on meeting 08.05.2013

ABSTRACT

TAMPERE UNIVERSITY OF TECHNOLOGY
Master's Degree Programme in Information Technology
LOULOU, ALAAEDDIN Y. M.: ENHANCED OFDM FOR FRAGMENTED SPECTRUM USE
Master of Science Thesis, 87 pages, 6 Appendix pages
October 2013
Major subject: Communications Engineering
Examiners: Prof. Markku Renfors, Dr. Juha Yli-Kaakinen
Keywords: Spectral shaping, OFDM, Cancellation carrier, Sidelobe suppression, LTE

OFDM, as a multiplexing and modulation scheme, transmits digital data on orthogonal, overlapped and non-interfering subcarriers saving spectral bandwidth. OFDM scheme offers high level of adaptivity through spectral fragmentation. Hence, each subcarrier can be modulated and coded independently according to the channel situation and users' requirements. Generally, the recent and emerging wireless systems have selected OFDM scheme due to its adaptivity. Besides, the advanced cognitive radio, dynamic spectrum use and fragmented coexistence scenarios consider OFDM as the first candidate technology to employ the available spectral gaps effectively for communications. Nevertheless, OFDM scheme leaks high power sidelobes in the unused part of the spectrum. This limits the spectral use near the active subcarriers. Therefore, several sidelobe suppression techniques are proposed in the literature to reduce sidelobe power, which is very important in advanced spectrum use concepts.

This thesis is in the context of sidelobe suppression in OFDM schemes, discussing four different suppression techniques, i.e., time domain windowing, cancellation carrier, subcarrier weighting and polynomial cancellation coding, which are investigated in details. Consequently, the four represented techniques are applied on a practical 5 MHz 3GPP LTE scenario. Finally, the required trade-offs for each technique are evaluated.

The target of this research is to properly elaborate the selected techniques for suppressing the sidelobes in contiguous and non-contiguous cases and without causing a severe side effects to the OFDM model. The contributions of this thesis include improvements to the edge windowing and cancellation carrier techniques, enhancing their suppression performance and reducing their limitations. Moreover, the improved methods are developed, showing an effective sidelobe suppression performance in both narrow gaps and on the guard bands of the OFDM signal.

PREFACE

This report is my master thesis for the conclusion of my Master's Degree Program in Information Technology in the field of communications engineering at the Faculty of Computing and Electrical Engineering, Tampere University of Technology, Finland. This work is carried out within and funded by the European Union FP7-ICT project EMPhAtiC under grant agreement no. 318362.

My supervisor in the project has been Professor Markku Renfors. And my first word of thanks, gratitude and appreciation goes to Professor Markku Renfors. Throughout the whole process of performing this thesis, Professor Renfors maintained a very professional and tactful attitude, which extremely motivated me to devote myself to this project in the best possible manner. Moreover, I would like to thank Dr. Juha Yli-Kaakinen for reviewing my thesis in an accurate and careful way.

Furthermore, I would like to thank my family and friends for being helpful and supportive during my time performing this research. And in the end, I would like to share a quote by Eric Butterworth:

"Do not go through life, grow through life."

Tampere University of Technology, Finland
October, 2013
AlaaEddin Loulou

TABLE OF CONTENTS

LIST OF FIGURES

LIST OF TABLES

LIST OF ABBREVIATIONS

1CC	1 cancellation carrier and 1 optimization point
1RB	1 resource block
2CC	2 cancellation carriers and 2 optimization points
2RB	2 resource blocks
3GPP	3rd Generation Partnership Project
BER	Bit Error Rate
CC	Cancellation carrier
CP	Cyclic Prefix
DFT	Discrete Fourier Transform
DTFT	Discrete Time Fourier Transform
FFT	Fast Fourier Transform
i.i.d.	Independent and identically distributed
ICI	Inter Carrier Interference
IDFT	Inverse Discrete Fourier Transform
IFFT	Inverse Fast Fourier Transform
ISI	Inter Symbol Interference
LLS	Linear Least Squares
LTE	Long Term Evolution
OFDM	Orthogonal Frequency Devision Multiplexing
PAPR	Peak to Average Power Ratio
PCC	Polynomial Cancellation Coding
PMR	Professional Mobile Radio
PSD	Power Spectral Density
PSK	Phase Shift Keying

QAM	Quadrature Amplitude Modulation
RB	Resource block
RC	Raised Cosine
S/P	Serial to parallel converter
SW	Subcarrier weighting
ZP	Zero Padding

LIST OF SYMBOLS

$\delta(...)$	The Dirac delta function
$\phi(t)$	Complex subcarrier
ω	Real angular frequency
$\mathcal{A}$	Number of real addition (or subtraction) operations per OFDM symbol
$\mathcal{C}$	Number of real multiplication operations per OFDM symbol
$\mathbf{C}$	CC's matrix
$\mathcal{D}$	Number of real division operations per OFDM symbol
$\mathbf{g}$	Weights vector
G	Number of edge technique groups
M	Number of CC's
mod(...)	Modulus operation
N	Number of subcarriers
N_{CP}	Length of CP in samples
N_{FFT}	FFT transform length
N_s	Length of CP-OFDM symbol in samples
N_u	Length of useful part of OFDM symbol in samples
N_w	Window length in samples
N_{wnd}	Windowed OFDM symbol length in samples
$O(...)$	Lower bound of worst-case complexity
$\mathbf{P}$	Sidelobes vector
P_{xx}	Power spectral density
q	The ratio of CP period to useful part period of OFDM symbol
S	Number of optimization points

$\mathcal{S}$	Number of real square root operations per OFDM symbol
S_{xx}	Energy spectral density
T	Sampling period
T_{CP}	Duration of CP
T_{CP}^{in}	CP period of inner group
T_{CP}^{ed}	CP period of edge group
T_s	Duration of CP-OFDM symbols
T_u	Duration of useful part of OFDM symbol
T_w	Duration of window
T_w^{ed}	Window period of edge group
T_w^{in}	Window period of inner group
T_{wnd}	Duration of windowed OFDM symbol
x_k	kth data sample in OFDM symbol
$y(t)$	Modulated OFDM symbol in time domain

1. INTRODUCTION

The ultimate goal of modern wireless communications is to be able to connect the mobile user anywhere and anytime using any data [1]. Therefore, the on-going research and standardization activities are trying to overcome the obstacles and enhance the use of wireless channel resources to support the heavily increasing traffic volume. However, the available spectral bandwidth at the desired time and place controls the ability of transmission. Hence, provisioning extra bandwidth is a major factor for achieving the ultimate wireless communications target.

Practical studies about the radio spectrum usage show that the licensed users don't use the service all time. Therefore, there is always unused bandwidth in the form of spectral gaps. To improve the efficiency of the spectrum use, the temporary gaps can be exploited by other users (unlicensed users) without interfering with the licensed users. In this context, the cognitive radio concept formulates the idea of exploiting spectral gaps in licensed spectrum to provision extra bandwidth [2]. Basically, cognitive radio model contains four basic features that guarantee the spectral efficiency. Firstly, the system can sense and recognize the empty gaps of the spectrum, i.e., spectral awareness. Secondly, the system has to shape the signal power, center frequency and bandwidth, i.e., spectral shaping. Thirdly the system has to be interoperable across the networks, in such a way that the users can roam between various systems. Fourthly, the system has to be adaptive, i.e., it should be able to learn and understand users' actions and decisions. At shorter sight, dynamic access networks and heterogeneous wireless system concepts are the path towards advanced cognitive radio concepts.

OFDM scheme shows high compatibility with the cognitive radio concept since the basic features of cognitive radio are integrated naturally in the OFDM scheme. Firstly, the OFDM spectrum is divided into equally spaced and orthogonal subcarriers. The orthogonality is maintained by using inverse fast Fourier transform (IFFT) and fast Fourier transform (FFT) at the transmitter and receiver, respectively. Thus, OFDM can shape the spectrum by simply deactivating the unused subcarriers. Secondly, the OFDM scheme simplifies the sensing operation since an FFT module is integrated in every OFDM receiver, i.e., FFT produces a frequency domain representation of the signal. Therefore, the required hardware for sensing process is reduced compared to single carrier schemes. Thirdly, many standards employ OFDM scheme

for wireless transmission, e.g., IEEE 802.11, digital audio broadcasting (DAB), digital video broadcasting (DVB), LTE 3GPP and WiMAX. Thus, interoperability can be achieved between different OFDM standards. Fourthly, OFDM system is able to modify the transmitted power, digital modulation and coding of each individual subcarrier according to channel quality or users' requirements. Besides, further adaptivity can be gained in OFDM scheme by changing the cyclic prefix (CP) length, subcarrier spacing, data subcarrier interleaving and pilots pattern according to the channel quality.

However, several obstacles face the cognitive radio implementation using the OFDM scheme. One of the major problems is OFDM spectral leakage. OFDM subcarriers leak continuous and relatively high powered sidelobes around the activated subcarriers. OFDM sidelobes introduce high interference level to users exploiting the empty spaces near active subcarriers. Therefore, spectral efficiency of OFDM is reduced since guard bands are required around the active spectrum. One important and interesting application of advanced opportunistic spectrum use concepts is the professional mobile radio (PMR) utilized by safety organizations [3]. There is a strong demand for broadband communication services by the safety organizations, and one basic approach for this is to try to fit them in the same frequency band with current narrowband PMR systems. The idea is to use the spectrum slots left unused by the existing systems for a new broadband system, the 3GPP LTE system being a strong candidate for this application. However, the spectral characteristics of LTE are not suitable for this application, and some enhancements in them would be needed.

Consequently, a lot off research has been carried out to develop methods for reducing the spectral sidelobes of the OFDM signal. The traditional way to suppress the sidelobes is to use filters. But filtering has relatively high computational complexity. Besides, it causes smearing between OFDM symbols in time domain. Hence, CP extension might be required to tolerate the resulting interference in filtering method [4]. A straightforward approach is reshaping OFDM symbols in time domain. This is called time domain windowing [5] and edge windowing [6] is its enhanced variant. Moreover, an effective suppression can also be achieved by inserting additional, properly weighted subcarriers. This is the so-called cancellation carrier (CC) technique [7]. Another method, called subcarrier weighting (SW), reduces the sidelobes by reweighting the subcarrier amplitudes by carefully optimized factors [8]. Furthermore, sidelobe suppression can be performed by precoding the OFDM signal as in the polynomial cancellation coding (PCC) technique [9]. Yet other methods proposed for sidelobe suppression, e.g., adaptive symbol transition [10], additive signal [11] and constellation expansion [12]. However, these sidelobe suppression techniques require a lot of compromises in terms of increased computa-

tional complexity, reduced in bit error rate (BER) and peak to average power ratio (PAPR) performance, losses in time domain resources and consequently, losses in the total throughput.

This thesis demonstrates the reasons that cause sidelobes in the OFDM spectrum analytically. The analytical way of representing the OFDM spectrum shows accuracy in power spectral density (PSD) plots, which is necessary to reveal the suppression performance of the sidelobe suppression techniques. The techniques selected for detailed investigations are time domain windowing, CC technique, SW and PCC. These techniques are chosen based on their reported effective suppression performance with acceptable compromises. The selected four techniques are investigated in a practical case study using the 5 MHz 3GPP LTE system as the basis. These methods are tailored to match the requirements of the considered radio access scenario, minimizing the possible side effects. Moreover, effective improvements are introduced to CC and edge windowing methods to reduce the related disadvantages, including detailed justifications for each modification. The performance of each technique is evaluated in comparison with the others, showing the effectiveness of each technique in different scenarios and CP modes of 5 MHz LTE. Then, the possible side effects are discussed in detail in terms of PAPR, BER, computational complexity, power consumption and resources usage.

The structure of this thesis is as follows: Chapter 2 develops the mathematical model of OFDM that is necessary to evaluate the PSD of different OFDM variants analytically in order to guarantee accurate results. Chapter 3 elaborates the used four techniques in details for the considered scenarios. Moreover, the implementation structure of each technique is depicted by showing the required computational complexity for each of them and the side effects of the methods are analyzed. Generally, the expected suppression performance of each technique is discussed. Chapter 4 focuses on the suppression performance of the four techniques in the 5 MHz 3GPP LTE scenario. Basically, the suppression performance is investigated in non-contiguous and contiguous scenarios with different CP modes. Furthermore, the proposed improvements to the techniques are justified carefully, showing their effect in different cases. A combination of two of the methods, with complementary characteristics, is proposed and shown to provide the best sidelobe suppression performance. Chapter 5 focuses on the possible side effects of the presented suppression techniques. Detailed comparative figures and tables show the properties of each technique in terms of PAPR, BER, power consumption, computational complexity and resource usage. The last chapter summarizes the results obtained by simulations, considering both the suppression performance and side effects. Moreover, the chapter lays down possible future research topics and ideas for future work.

2. THEORETICAL BACKGROUND

This chapter lays the basic concepts and groundwork used in this document. In Section 2.1, the basic OFDM model is explained, focusing on main OFDM foundations, which are orthogonality, IFFT/FFT implementation and the use of CP. Meanwhile, the general mathematical formulation of OFDM scheme is concluded as these formulas are essential for deriving the spectral representation of the OFDM scheme. Besides, the general advantages and disadvantages of OFDM scheme are argued. Section 2.2 introduces PSD estimation techniques that can be used for deriving OFDM frequency representation, showing the benefits and drawbacks associated with each PSD estimation technique. Finally, the most accurate PSD estimation technique, to be used throughout this document, is formulated and the PSD of the basic CP-OFDM scheme is illustrated.

2.1 OFDM overview

OFDM scheme is a multicarrier technique that fragments the spectrum into equally spaced orthogonal overlapping subcarriers. The orthogonality eliminates the interference between the overlapping subcarriers resulting in an enhancement of the spectral efficiency. OFDM scheme maintains the orthogonality by using IFFT/FFT block for modulation and demodulation. The usage of IFFT/FFT block simplifies the equalization process and reduces the computational complexity of OFDM scheme [13]. Furthermore, OFDM scheme offers an effective and simple way to eliminate inter symbol interference (ISI) and multipath effects by using CP [14]. However, the basic OFDM scheme still experiences various drawbacks that limit its applicability in difficult application scenarios.

2.1.1 OFDM model and orthogonality

Basically, the OFDM scheme modulates a set of parallel symbols to orthogonal subcarriers. Therefore, lets assume that we have a set of random independent and identically distributed (i.i.d.) complex parallel data samples $\{x_0, x_1, ..., x_{N-1}\}$, where N is the number of subcarriers and T_u is the useful duration of OFDM symbols. Then OFDM modulates these data samples to complex subcarriers $\phi(t) = \exp[j2\pi f_k t]$.

The resulting modulated subcarrier is:

$$y_k(t) = x_k \exp[j2\pi f_k t]. \tag{2.1}$$

Hence, the modulated OFDM symbol is the sum of N frequency shifted subcarriers that are weighted by data samples x_k. The modulated OFDM symbol is expressed as follows:

$$y(t) = \sum_{k=0}^{N-1} x_k \exp[j2\pi f_k t]. \tag{2.2}$$

The frequency shifts between subcarriers must be defined properly to achieve orthogonality. Orthogonality is the mathematical relation between two functions where their inner product over certain interval is zero [15], i.e., the functions do not interfere with each other in that specific interval. In the OFDM scheme, maintaining orthogonality suppresses interference between subcarriers in the used spectral range and between consecutive symbols in time domain. Therefore, orthogonality eliminates the need for guard bands between subcarriers [16]. The orthogonality relation is expressed in the following way:

$$\langle f_m, f_n \rangle = \int_a^b f_m^*(x) f_n(x)\, dx = 0 \text{ if } m \neq n. \tag{2.3}$$

Accordingly, the OFDM orthogonality condition is found as follows:

$$\begin{aligned} \langle y_k, y_l \rangle &= \int_0^{T_u} y_k^*(t) y_l(t)\, dt \\ &= \int_0^{T_u} x_k^* \exp[-j2\pi f_k t] x_l \exp[j2\pi f_l t]\, dt \\ &= x_k^* x_l \int_0^{T_u} \exp[j2\pi t(f_l - f_k)]\, dt \\ &= x_k^* x_l [\frac{\exp[j2\pi T_u(f_l - f_k)] - 1}{j2\pi(f_l - f_k)}]. \end{aligned} \tag{2.4}$$

Equation (2.4) shows that if $(f_l - f_k)2\pi T_u = 2m\pi$, where m is an integer, then $\langle y_k, y_l \rangle$ equals 0. As a result, the orthogonality condition for OFDM subcarriers is expressed in the following way:

$$f_l - f_k = \frac{m}{T_u}. \tag{2.5}$$

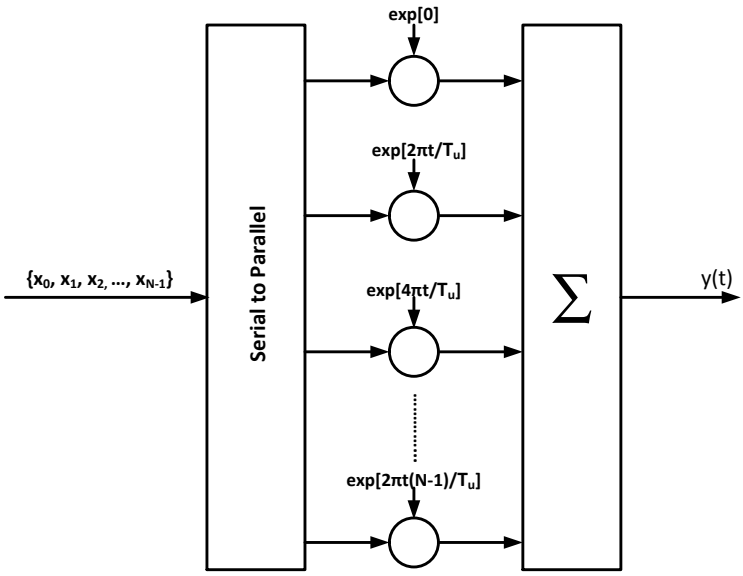

Figure 2.1: Basic implementation of OFDM scheme.

The expression proves that OFDM orthogonality can be achieved, if the frequency spacing of the subcarriers equals $1/T_u$. This is the smallest possible frequency spacing resulting in the highest spectral efficiency. Accordingly, substituting $f_k = k/T_u$ in Equation (2.2), an OFDM symbol can be expressed in the following way:

$$y(t) = \sum_{k=0}^{N-1} x_k \exp[j2\pi tk/T_u]. \tag{2.6}$$

To obtain the corresponding discrete time expression for OFDM symbol, we substitute $t = nT$ and $T_u = NT$ in Equation (2.6), where T is the sampling period and n is the discrete time index. The resulting discrete time of OFDM symbol is expressed as follows:

$$y(nT) = \sum_{k=0}^{N-1} x_k \exp[j2\pi nk/N]. \tag{2.7}$$

Consequently, OFDM symbol generation can be implemented as shown in Figure 2.1. The system consists of serial-to-parallel (S/P) converter, after which the subcarrier symbols x_k are modulated to subcarriers at multiples of $1/T_u$. Finally, all modulated symbols are summed to form an OFDM symbol.

2.1.2 OFDM scheme based on IFFT/FFT

One of the attractive advantages of OFDM scheme is that it can be implemented efficiently using IFFT and FFT blocks. Basically, IFFT and FFT are algorithms that are used to compute inverse discrete Fourier transform (IDFT) and discrete

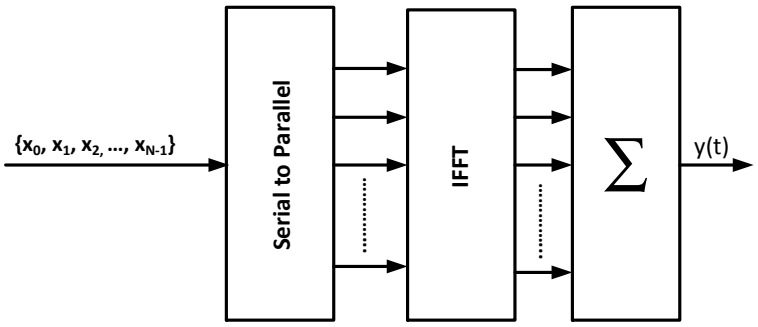

Figure 2.2: The implementation of OFDM scheme using IFFT block.

Fourier transform (DFT) quickly and efficiently, in the following way:

$$y_n = \sum_{k=0}^{N_{FFT}-1} X_k \exp[j2\pi kn/N_{FFT}] \tag{2.8}$$

$$X_k = \sum_{n=0}^{N_{FFT}-1} y_n \exp[-j2\pi kn/N_{FFT}]. \tag{2.9}$$

Here Equations (2.8) and (2.9) are the mathematical expressions of IDFT and DFT, respectively [17], and N_{FFT} denotes the transform length. By comparing Equations (2.7) and (2.8), the two formulas match when $N_{FFT} = N$. Accordingly, an IDFT block can be used as an OFDM modulator. However, the computational complexity of IDFT block is high as it is proportional to $O(N^2)$ operations. Therefore, using effective implementation algorithms, IFFT/FFT, instead reduces the system complexity as IFFT/FFT blocks require $O(N \log N)$ operations [18]. The OFDM scheme based on IFFT/FFT can be implemented as shown in Figure 2.2. The new implementation replaces the complex exponential multipliers by IFFT block. This results in the same output as the structure of Figure 2.1 but with greatly reduced computational complexity.

2.1.3 Cyclic prefix

Multipath propagation is a destructive effect that is generated by summing delayed versions of the signal to the original one due to signal reflections and diffractions during signal propagation in the radio channel. In fact, multipath yields unwanted phenomenon called ISI. The effect of ISI appears as dispersion of the symbol pulses resulting in neighboring symbols to overlap with each other. The existence of ISI introduces errors to decisions made at receiver side and reduces the system throughput. In the OFDM scheme, the multipath effect seems to be more destructive; when the data symbols interfere with their neighbors, OFDM symbols lose their orthogonality. Therefore, the concept of CP is introduced as a robust solution to mitigate

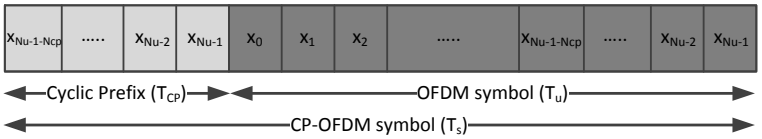

Figure 2.3: The structure of CP-OFDM symbol in time domain.

the multipath channel effects in OFDM systems. CP refers to an extra sequence of samples appended to the beginning of the OFDM symbol.

Figure 2.3 shows the OFDM symbol structure in time domain, where the original data symbols are colored with dark gray and the copied data symbols are colored with light gray. The new extension of duration T_{CP} is copied from the end of the OFDM symbol increasing the total OFDM symbol duration to $T_s = T_u + T_{CP}$. The new generated symbol is denoted as CP-OFDM symbol. Then, the CP-OFDM symbol can be expressed in the following form:

$$y(t) = \sum_{k=-N_{CP}}^{N-1} x_{\mathrm{mod}(k,N-1)} \exp[j2\pi t \,\mathrm{mod}(k, N-1)/T_u], \tag{2.10}$$

where N_{CP} is the number of cycled data samples. The total length of the CP-OFDM symbol is defined as $N_s = N_u + N_{CP}$ samples.

The time period of CP length, T_{CP}, has to be equal to or longer than the maximum channel delay spread in order to eliminated the ISI. If the condition is satisfied, then the required equalization to compensate the channel distortion is reduced to one complex multiplier in each subcarrier [14]. Nevertheless, the CP reduces the overall throughput of OFDM model as longer time period is required for transmitting the same amount of data. Besides, CP has a slight impact on the OFDM spectrum as it produces ripples in the useful range [19]. This impact is discussed in details in Subsection 2.2.2.

2.1.4 OFDM system advantages and challenges

The OFDM scheme is preferred over conventional single carrier transmission due to its distinct advantages. It shows robustness against multipath fading since the spectral fragmentation used in OFDM simplifies channel equalization by using single bank of complex multipliers with the help of CP. In other words, the concept of CP introduces a simple technique to eliminate ISI. Additionally, OFDM scheme is implemented with low complexity using IFFT/FFT blocks, which maintains OFDM orthogonality efficiently. The orthogonality in OFDM allows overlapping between subcarriers without causing interference. As a result, guard bands are not required between subcarriers. Subsequently, frequency resources are saved, improving the spectral efficiency of the OFDM scheme. Besides, the spectral fragmentation pro-

vides transmission flexibility and adaptivity, e.g., the used modulation and coding techniques can be varied among the subcarriers according to the channel requirements of each user.

However, the OFDM scheme has also some drawbacks that are originated from the non-ideal OFDM implementation and others are due to the communication channel impact on the OFDM signal.

In the ideal OFDM spectrum, infinite ripples called sidelobes are leaked around the useful part of the OFDM spectrum, see Figure 2.5. The sidelobes contain a relatively high power particularly at sidelobes close to active subcarriers. To avoid interference, guard bands are added around OFDM active subcarriers to keep the neighboring channels away from the high power sidelobes. This reduces the OFDM spectral efficiency. OFDM sidelobes are generated because of the OFDM symbol shape. Commonly, OFDM symbols are considered as multiplied by rectangular function in time domain, which results in convolution with sinc function in frequency domain. Further discussions on this issue are included in Subsection 2.2.2.

The high peak-to-average power ratio (PAPR) is another problem that exists in the OFDM scheme. Normally, OFDM scheme produces high PAPR, because of the implementation nature of the OFDM symbol. As mentioned in Equation (2.6), OFDM symbol is the sum of samples values multiplied by complex exponentials. A complex exponential is the sum of a real cosine and imaginary sine wave. At some moments, the cosines and sines sum up to produce a high peak compared to the RMS value of the OFDM symbol. High PAPR requires high linearity in transmitter's amplifiers since high peaks are saturated in nonlinear amplifiers, causing intermodulation products in the OFDM spectrum. There are different techniques presented in the literature to mitigate this problem, e.g., Tone Reservation, Tone Injection and Partial Transmit Sequence [20].

Another drawback is the high sensitivity to frequency and time offsets. Therefore, a highly accurate synchronization process is needed for the OFDM scheme. The source of the time and frequency errors is different but both are caused by channel effects and transmitter and receiver non-idealities. Time synchronization is needed at the receiver side in order to identify the first symbol in the transmitted OFDM signal. Timing error impact appears as phase rotation of the subcarriers. As long as time delay spread is shorter than the CP length, the OFDM scheme can estimate and compensate the timing error. But if the timing error makes the maximum excess delay to exceed the CP length, this leads to loss of subcarrier orthogonality and degradation of BER performance. Basically, there are two main approaches for estimating the timing offset, based on pilot symbols or the CP structure [14]. Frequency offset is the frequency difference between the carrier frequency of the received signal and the receiver's local oscillator signal. It is caused by inaccuracy of

the local oscillators and by the Doppler shifts due to transmitter or receiver movements. The frequency offset results in frequency shifts in subcarriers. Frequency shifts make the received subcarrier signals affected by neighboring subcarriers. This effect denoted as inter carrier interference (ICI). To eliminate the frequency errors, several techniques have been proposed using pilots or CP [14].

2.2 OFDM power spectral density estimation

Since the sidelobe problem exists in the frequency domain, spectrum analysis is a critical issue for OFDM sidelobe suppression studies. In fact, there are various techniques used to estimate the signal power spectrum. Nevertheless, these techniques have different levels of accuracy. In this study, the accuracy of PSD evaluation technique is justified in order to be exploited in the evaluation of the performance the suppression techniques.

2.2.1 Power spectral density estimation

Basically, the PSD describes the power distribution versus frequency. Power is defined as the average energy over time. Accordingly, PSD can be defined as the average of energy spectral density over time period $T \to \infty$ at ω. Energy spectral density is defined as the mean squared value of the signal representation in frequency domain $X(\omega)$. The mathematical expression for energy spectral density and PSD are expressed as follows:

$$S_{xx}(\omega, T) = E[|X(\omega, T)|^2] \tag{2.11}$$

$$P_{xx}(\omega) = \lim_{T\to\infty} \frac{S_{xx}(\omega, T)}{T} = \lim_{T\to\infty} \frac{E[|X(\omega, T)|^2]}{T}, \tag{2.12}$$

respectively. Here, it is possible to apply those formulas also on discrete time signals [21], in which case the time period, T, must be substituted by the number of samples, N.

In Equation (2.12), where $X(\omega, T)$ is the frequency domain representation of the signal, frequency transformation is a critical factor for the PSD estimation. Fourier transform is used to represent the spectrum of a continuous-time signal. Besides, discrete time Fourier transform (DTFT) and DFT are used for representing discrete-time signals in frequency domain.

In practice, OFDM is implemented using discrete-time signal processing. Therefore, it is possible to use DFT or DTFT to evaluate its spectrum. Accordingly, let's first examine the accuracy of DTFT and DFT which are the common choices for spectrum estimation of digital signals. DTFT represents the discrete signal x_n in terms of exponential sequences of continuous frequency, $\exp[-j\omega n]$. DTFT is

calculated in the following way:

$$Y(\mathrm{e}^{j\omega}) = \sum_{n=-\infty}^{\infty} x_n \exp[-j\omega n], \tag{2.13}$$

where ω is the real angular frequency [17]. DTFT always results in a periodic continuous function of period 2π. DFT can be considered as discrete version of DTFT. In fact, DFT is obtained from DTFT by sampling it at N_{FFT} equally-spaced points, such that the spacing between two consecutive frequencies is $2\pi/N_{FFT}$.

A finite-length signal can always be multiplied by rectangular window. This rectangular window has a width of T_u and amplitude of unity. The rectangular function is represented as $\frac{\sin(\pi f)}{\pi f}$ or $\frac{\sin(\omega N/2)}{\sin(\omega/2)}$ in frequency domain, using Fourier transform and DTFT, respectively. Therefore, the spectrum for any time limited signal is the convolution of the spectra of the unlimited form of the signal and the rectangular window.

DFT does not have different spectrum realization than DTFT, whilst DFT is considered as a frequency representation of periodic time signal with period N. This means that DFT looks to the limited sequence in time domain as it is repeated infinitely. Therefore, if the window length is not equal to the signal period or its multiple, the resulting spectrum contains so-called leakage phenomenon [22]. In case of perfect periodicity, the locations of DFT bins are the same as the positions of signal frequency components on frequency axis. Therefore, the resulting spectrum does not contain any problem. Yet, this is not frequent occurring case. Frequently the frequency bins are not located at signal's frequency components because of signal discontinuity between signal ends. Therefore, the resulting frequency bins contain energy accumulated or leaked from neighboring frequency components. Clearly, increasing the number of DFT points (improving frequency resolution) reduces the effect of leakage, since extra frequency bins will hit or get closer to the original frequency components of the signal.

Figure 2.4 shows two cases of sine wave. The first case is a well contained sine wave in the rectangular window where the end of sine wave is connected to its beginning in Figure 2.4(a). Hence, the resulting spectrum in Figure 2.4(b) contains only two impulses without any leakage. The second case is a discontinuity between the end and the beginning of the sine wave, i.e., the period of the sine does not match with the transform length in Figure 2.4(c). The resulting spectrum in Figure 2.4(d) contains many peaks which are far away from the true spectrum in Figure 2.4(b).

In this document, more detailed discussion of DFT usage for estimating PSD will be skipped although there are various techniques to reduce the PSD estimation variance, e.g., Welch method [23] and Bartlett method [24]. Instead of that, continuous

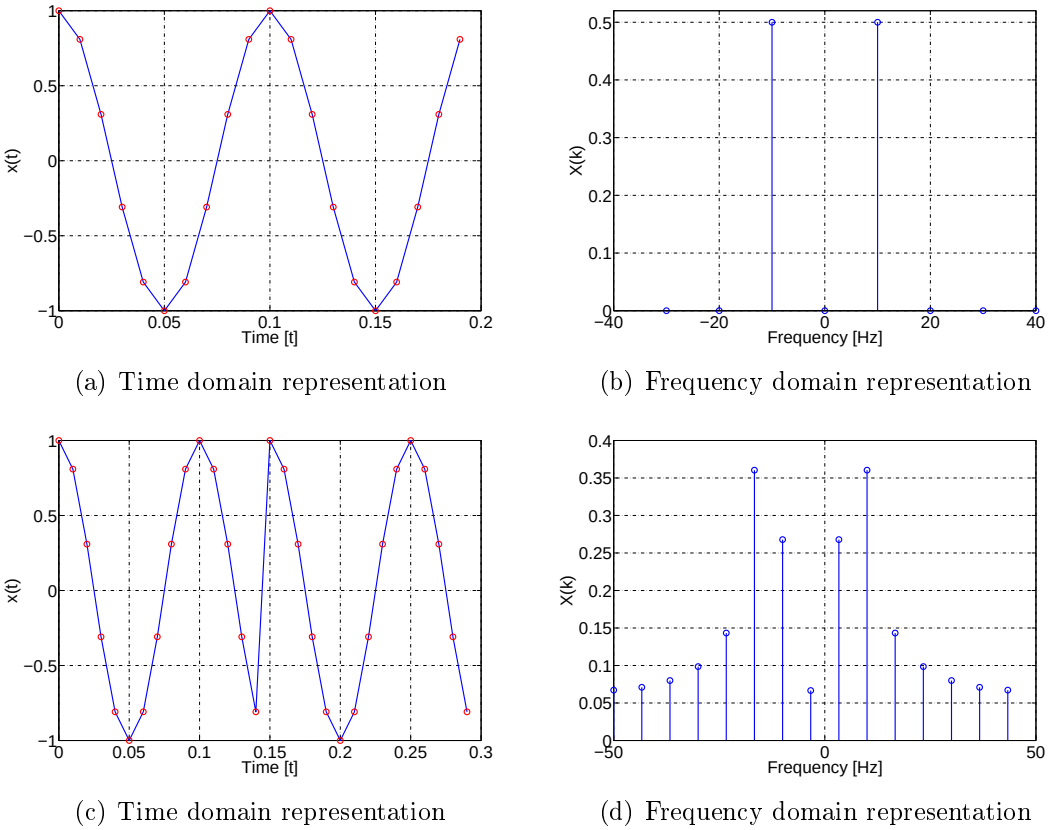

(a) Time domain representation

(b) Frequency domain representation

(c) Time domain representation

(d) Frequency domain representation

Figure 2.4: Two periods of a 10 Hz discrete-time sine signal at 100 Hz sampling rate corresponding to 10-points DFT in (a) & (b) and 15-points DFT in (c) & (d).

frequency representation is more reliable and accurate for PSD estimation purposes. Thus, analytical modeling and Fourier transform is used for OFDM spectral analysis and simulations in the following sections.

2.2.2 OFDM spectrum estimation

The spectral analysis of OFDM schemes require a careful examination of the specifics of the OFDM implementation. In Figure 2.2, the (S/P) block divides the signal into parts of equal lengths forming the OFDM symbols. Consequently, the (S/P) block feeds the IFFT block with phase shift keying (PSK) or quadrature amplitude modulation (QAM) modulated symbols. It is essential in OFDM spectral studies to define these divisions mathematically as the modulated OFDM symbol multiplied by the time-shifted rectangular window. Accordingly, the mathematical expression of OFDM scheme in Equation (2.6) has to be updated in order to consider the rectangular window as follows:

$$y(t) = \sum_{c=0}^{\infty} \left[\sum_{k=0}^{N-1} x_{k,c} \exp[j2\pi k(t - cT_u)/T_u] \right] \text{rect}\left[\frac{t - cT_u}{T_u} \right]. \tag{2.14}$$

Consequently, the Fourier transform of OFDM signal is evaluated in the following way:

$$\begin{aligned} Y(f) &= \sum_{c=0}^{\infty} T_u \exp[j2\pi f T_u c] \left[\sum_{k=0}^{N-1} x_{k,c} \delta \left[f - \frac{k}{T_u} \right] \right] * \operatorname{sinc}[f T_u] \\ &= T_u \sum_{c=0}^{\infty} \exp[j2\pi f T_u c] \sum_{k=0}^{N-1} x_{k,c} \operatorname{sinc}[f T_u - k], \end{aligned} \tag{2.15}$$

where $\operatorname{sinc}(x) = \frac{\sin(\pi x)}{\pi x}$. Then, the PSD can be derived by applying Equation (2.12) directly or it can be simplified if $x_{k,c}$ is i.i.d. to the following expression [25]:

$$P_y(f) = T_u \sum_{k=0}^{N-1} E[|x_{k,c}|^2] \left| \operatorname{sinc}[f T_u - k] \right|^2. \tag{2.16}$$

Obviously, Equations (2.15) and (2.16) contain shifted and weighted sinc functions. Each shifted sinc represents one subcarrier. In fact, the sinc function produces infinite ripples around its center. Thus, OFDM subcarriers interfere with each other, which explains the need for the orthogonality between the subcarriers. By maintaining the OFDM orthogonality, the generated ripples intersect frequency axis at center frequencies of the other subcarriers resulting in no interference in the useful range. However, subcarriers' ripples accumulate outside the useful band to generate a relatively high power ripples. Thus, OFDM sidelobes reduce the spectral efficiency so that other transmitters have to keep spectral space away from OFDM useful part in order to avoid interference. In multi-user operation, the orthogonality of OFDM subcarriers is maintained only if the subcarriers are precisely frequency synchronized and the relative timing differences can be absorbed by the CP, together with the channel delay spreads. This is called quasi-synchronous operation.

Figure 2.5 shows an example of the subcarriers' contributions to OFDM spectrum for $N = 30$ with $N_u = 10$ active subcarriers. Each subcarrier produces continuous ripples interfering with the neighboring subcarriers. Apparently, ripples cross zero at the points where the peaks of the other subcarriers are located. Outside the useful range, the ripples leak continuously causing interference.

CP spectral effect

The previous expressions in Equations (2.14), (2.15) and (2.16) neglect the effect of adding CP to the OFDM symbols. In fact, CP extends the rectangular function duration from T_u to T_s; hence, time domain representation in Equation (2.14) is

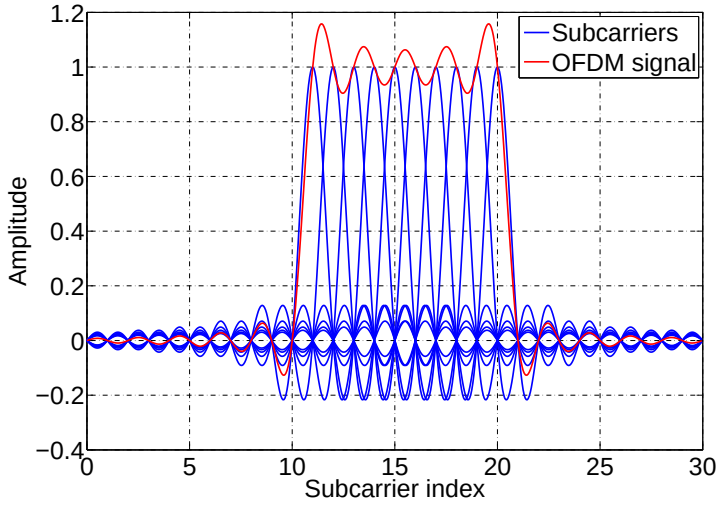

Figure 2.5: Orthogonal subcarriers behavior in OFDM spectrum.

updated as follows:

$$y(t) = \sum_{c=0}^{\infty} \left[\sum_{k=-N_{CP}}^{N-1} x_{\mathrm{mod}(k,N-1),c} \exp[j2\pi \mathrm{mod}(k, N-1)(t - cT_s)/T_u] \right] \mathrm{rect}\left[\frac{t - cT_s}{T_s} \right]. \tag{2.17}$$

Since the data samples of CP are copied data, their frequency components are contained in the interval $[0, k]$. Consequently, the OFDM spectrum is evaluated in the following way:

$$\begin{aligned} Y(f) &= \sum_{c=0}^{\infty} T_s \exp[j2\pi f T_s c] \left[\sum_{k=0}^{N-1} x_{k,c} \delta \left[f - \frac{k}{T_u} \right] \right] * \mathrm{sinc}\left[f T_s \right] \\ &= T_s \sum_{c=0}^{\infty} \exp[j2\pi f T_s c] \sum_{k=0}^{N-1} x_{k,c} \mathrm{sinc}\left[T_s \left(f - \frac{k}{T_u} \right) \right]. \end{aligned} \tag{2.18}$$

If $x_{k,c}$ is i.i.d., then the PSD is expressed as follows:

$$P_y(f) = T_s \sum_{c=0}^{\infty} \sum_{k=0}^{N-1} E[|x_{k,c}|^2] \left| \mathrm{sinc}\left[T_s \left(f - \frac{k}{T_u} \right) \right] \right|^2. \tag{2.19}$$

Let $q = \frac{T_{CP}}{T_u}$, then $\frac{T_s}{T_u} = 1 + q$. The Equation (2.19) can be rewritten to the following form:

$$\begin{aligned} P_y(f) = T_s \sum_{c=0}^{\infty} \sum_{k=0}^{N-1} E[|x_{k,c}|^2] |\mathrm{sinc}\left[(T_u f - k) \right] \frac{\cos\left[q\pi \left(T_u f - k \right) \right]}{1+q} \\ + \frac{\cos\left[\pi \left(T_u f - k \right) \right]}{(1 + 1/q)} \mathrm{sinc}\left[q \left(T_u f - k \right) \right] |^2. \end{aligned} \tag{2.20}$$

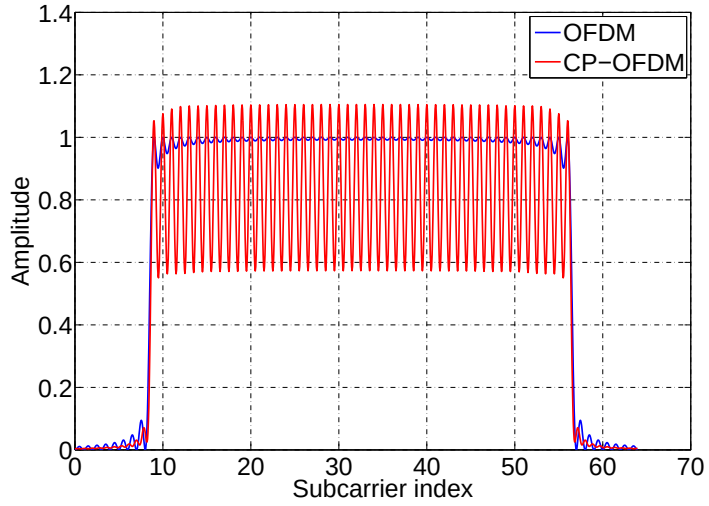

Figure 2.6: Spectrum of OFDM and CP-OFDM, for $N = 64$, $N_u = 48$ and $N_{CP} = 12$.

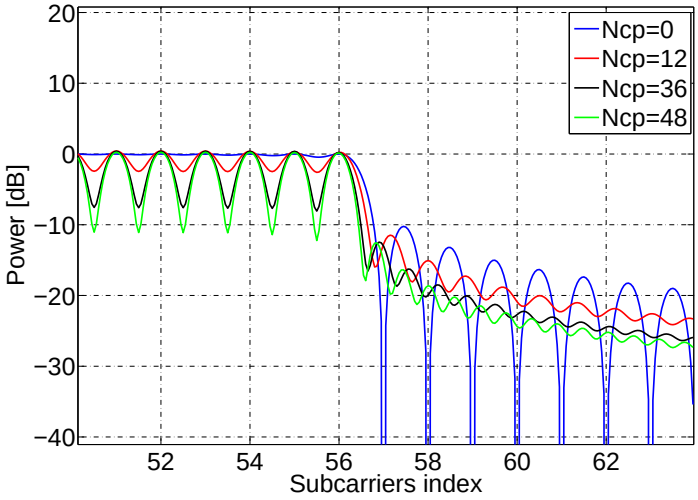

Figure 2.7: Spectrum of OFDM and CP-OFDM with different values of CP, for $N = 64$ and $N_u = 48$.

As a result, the CP changes the zero intersections of the sinc function. In Equations (2.15) and (2.16), the sinc function intersects zero at frequencies of $\frac{i+k}{T_u}$, where k is the subcarrier index and i is a positive integer. Therefore, subcarriers do not overlap with each others at subcarriers center frequencies. Whilst in Equations (2.17) and (2.18), the sinc function intersects zero at frequencies of $\frac{i}{T_s} + \frac{k}{T_u}$. The zero intersections go faster with rate of $\frac{1}{T_s}$, that results in an overlapping between subcarriers' center frequencies at $\frac{1}{T_u}$. The overlapping between subcarriers affects OFDM orthogonality, but this impact is simply removed at the receiver when the CP is removed. In Equation (2.20), the cosine factor changes the position of sidelobe peaks of OFDM spectrum, i.e, at the middle between two subcarrier centers, the value changes by the additional term $\frac{\cos[q\pi(T_u f - k)]}{1+q}$.

Figure 2.6 shows the spectrum of OFDM when CP is excluded versus CP-OFDM spectrum. Useful part of CP-OFDM spectrum contains strong ripples generated due to subcarriers overlapping. Figure 2.6 shows the OFDM spectrum with different lengths of CP. The amount of power increased in subcarriers centers is 0.2 dB, 0.4 dB and 0.4 dB when N_{CP} equals 12, 36 and 48, respectively. Hence, the effect of subcarrier overlapping can be negligible considering channel effects and added white noise. On other hand, CP-OFDM shows reduction in sidelobes with shifts in peaks of the sidelobes. The increase of the CP length results in increasing the variation at generated ripples in the useful band.

There is an alternative case of guard interval, which is the zero padding (ZP) case. In a ZP-OFDM system, the guard interval is filled with zeros instead of cycled data samples. Therefore, the signal is multiplied with a rectangle of width T_u. As a result, the spectrum of ZP-OFDM scheme is similar to the case of OFDM without CP. Thus, Equations (2.15) and (2.16) are valid to represent ZP-OFDM case. However, the normalization factor T_u has to be replaced by T_s to consider the time extension.

3. OFDM SIDELOBE SUPPRESSION TECHNIQUES

The highly powered sidelobes limit the spectral usage around active subcarriers. However, several studies have been published, proposing various techniques to suppress the OFDM sidelobes. Intuitively, to suppress OFDM sidelobes, additional processes are required to be included to the OFDM implementation. In this chapter, four common techniques for OFDM sidelobe suppression are discussed in detail, showing their basic ideas, mathematical formulations, implementations and performance. The techniques are evaluated according to their suppression performance and simplicity. Besides, various improvements are introduced.

3.1 Time domain windowing

The main reason for OFDM sidelobes is the rectangular shape of OFDM symbols in time domain. Unfortunately, this shape produces a sum of sinc functions in frequency domain. Therefore, the sum of sinc sidelobes accumulates to result in high powered sidelobes. Time domain windowing technique intends to suppress OFDM sidelobes by modifying the OFDM symbol shape directly. This modification adds a slope to OFDM symbol edges making the transition of the OFDM symbol longer and smooth. This transition is added by multiplying extended OFDM symbol in time domain with appropriate window that provides the smoothness needed in OFDM symbol [5]. Time domain windowing must not be confused with common frequency domain windowing; in this document windowing always refers to windowing in time domain. The main benefit of adding longer transitions to OFDM symbols is that it reduces the spectral power leakage of the OFDM scheme.

The window cannot be chosen in arbitrary way; there are some condition that has to be satisfied. Firstly, the window transition length has to be chosen according to the available time resources. Secondly, the window must not modify the values of original data samples in OFDM symbol. Hence, extra cycled data symbols have to be appended to the beginning (pre-window interval) and to the end (post-window interval) of the OFDM symbol as depicted in Figure 3.1. In order to decrease time losses, two consecutive OFDM symbols are allowed to interfere in pre-window and post-window intervals as shown in Figure 3.2. We refer to that period as window period of length N_w samples or T_w seconds such that the overall OFDM symbol

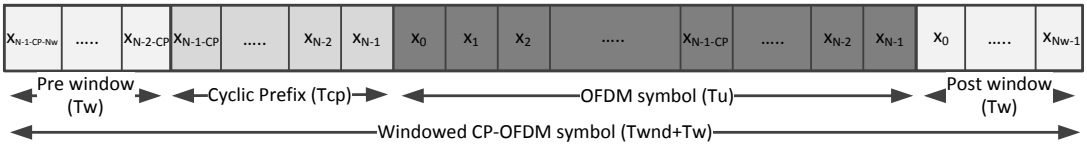

Figure 3.1: Windowed CP-OFDM symbol structure in time domain.

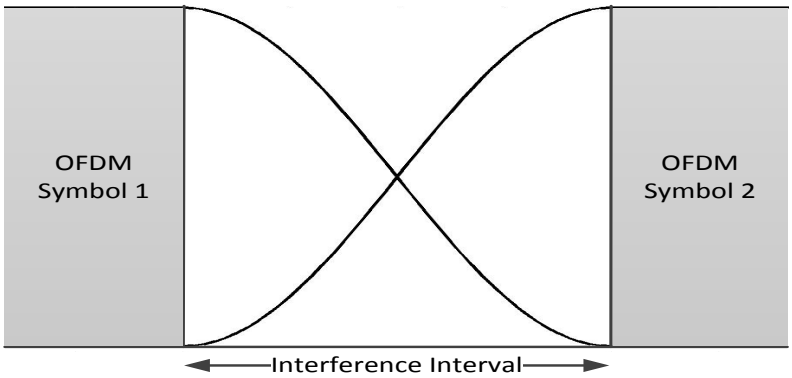

Figure 3.2: Interference interval between two consecutive windowed CP-OFDM symbols.

interval becomes $N_{wnd} = N_u + N_{CP} + N_w$ or $T_{wnd} = T_s + T_w$. Windowing modifies OFDM PSD in Equation (2.16). The PSD of windowed-OFDM can be expressed as follows:

$$P_y(f) = \sum_{k=0}^{N-1} E[|x_{k,c}|^2] \left| \mathrm{W}\left(f - \frac{k}{T_u}\right) \right|^2, \tag{3.1}$$

where $\mathrm{W}(f)$ is the frequency domain representation of window $\mathrm{w}(t)$ which has time duration of $T_{wnd} + T_w$.

Raised Cosine (RC) window (also known as tapered cosine window or Tukey window) is an appropriate shape for time domain windowing as it provides a controllable smoothness to windowed OFDM symbol without changing data symbol or CPs in time domain. RC window is expressed according to the following formula:

$$w_{RC}(t) = \begin{cases} \frac{1}{2} + \frac{1}{2}\cos\left(\pi + \frac{\pi t}{\alpha T_{wnd}}\right) & \text{for } 0 \le t < \alpha T_{wnd} \\ 1 & \text{for } \alpha T_{wnd} \le t < T_{wnd} \\ \frac{1}{2} + \frac{1}{2}\cos\left(\frac{\pi(t - T_{wnd})}{\alpha T_{wnd}}\right) & \text{for } T_{wnd} \le t < (1+\alpha) T_{wnd} \end{cases}, \tag{3.2}$$

where α denotes the roll-off factor that controls the length of window interval with $T_w = \alpha T_{wnd}$ [5]. The frequency domain representation of RC window is expressed in the following way:

$$W_{RC}(f) = T_s \mathrm{sinc}(f T_s) \left[\frac{\cos(\pi \alpha T_{wnd} f)}{1 - 4\pi^2 T_{wnd}^2 f^2} \right]. \tag{3.3}$$

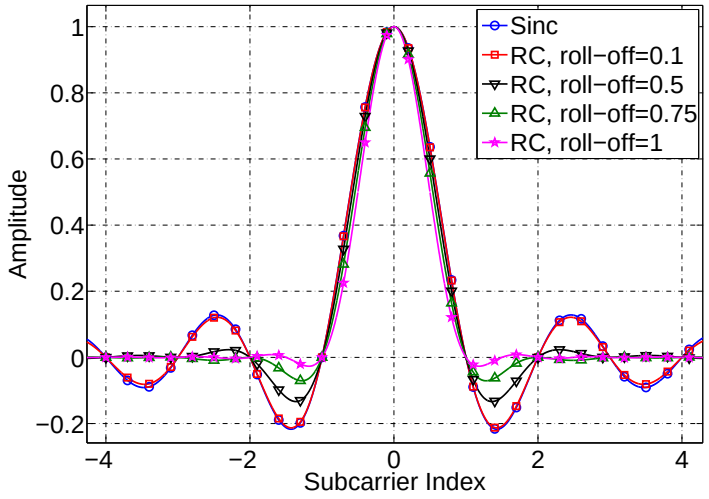

Figure 3.3: Sinc and RC function behavior at frequency domain.

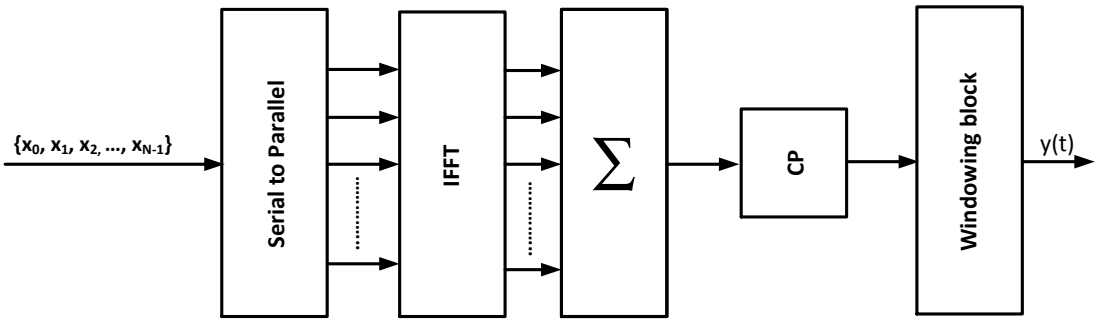

Figure 3.4: The implementation of windowed CP-OFDM model.

The RC window in frequency domain is a sinc function multiplied by the factor $\frac{\cos(\pi\alpha T_{wnd}f)}{1-4\pi^2T_{wnd}^2f^2}$ which reduces the sinc sidelobes. Figure 3.3 illustrates the reduction in the sidelobes of RC with increasing roll-off factor. In the sinc case, the first sidelobe is at the level of -13.3 dB while with a roll-off value of 0.5 it is at -17.5 dB. For the second sidelobe, the corresponding values are -17.8 dB and -32.7 dB, respectively. However, with the roll-off of 0.5, $T_w = T_{wnd}/2$, which means that half of the symbol period is reserved for sidelobe control. Hence, the trade-off between time overhead and suppression performance has to be carefully considered.

Figure 3.4 depicts the implementation model for windowed CP-OFDM. The CP operation is modified in a way that it appends cycled data in window interval. Then, an additional windowing block is added for multiplying each data symbol in the window interval with the RC coefficients of Equation (3.2). Figure 3.5 shows the detailed structure of the windowing block where the post-window of the previous CP-OFDM symbol is stored. Then, it is summed with the pre-window of the current CP-OFDM symbol generating the required interference window interval. Consequently, post-window of the current CP-OFDM symbol is stored to repeat the procedure

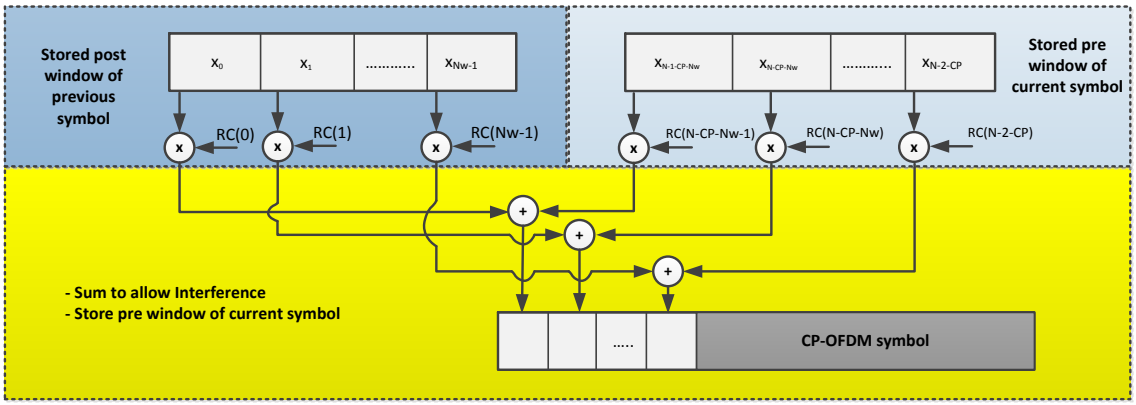

Figure 3.5: The structure of window block.

with the next CP-OFDM symbol.

Accordingly, the added computational complexity can be defined as follows:

$$\begin{aligned} \mathcal{C} &= 2N_w \\ \mathcal{A} &= N_w \end{aligned}, \tag{3.4}$$

where $\mathcal{C}$ is the number of real multiplication operations per OFDM symbol and $\mathcal{A}$ is the number of real addition (or subtraction) operations per OFDM symbol. The resulting computational complexity shows a linear increase which is proportional to window interval length N_w. Therefore, the added computational complexity of time domain windowing is relatively low compared to other proposed sidelobe suppression techniques. However, time domain windowing induces loss in the throughput due to extended symbol period and loss in power efficiency due to the energy transmitted during the transition intervals [26].

In general, RC time domain windowing results in significant sidelobe suppression performance, especially at sidelobes located far away from OFDM edges. In fact, the suppression performance increases as sidelobe location is getting farther away from the useful band of OFDM. Nevertheless, the suppression performance of time domain windowing on sidelobes close to useful band edges is considerably low.

Edge windowing

Edge windowing is an enhanced variant of time domain windowing where different windowing lengths are applied on different groups of subcarriers. Basically, subcarriers closer to the band edges leak power to sidelobes more than inner subcarriers. Therefore, edge windowing technique divides subcarriers to more than one group, usually two. Then, it applies different windows with different lengths to each group. Longer window is applied on edge group and shorter window is applied on inner groups [6]. The corresponding RC window lengths are denoted as T_w^{ed} and T_w^{in},

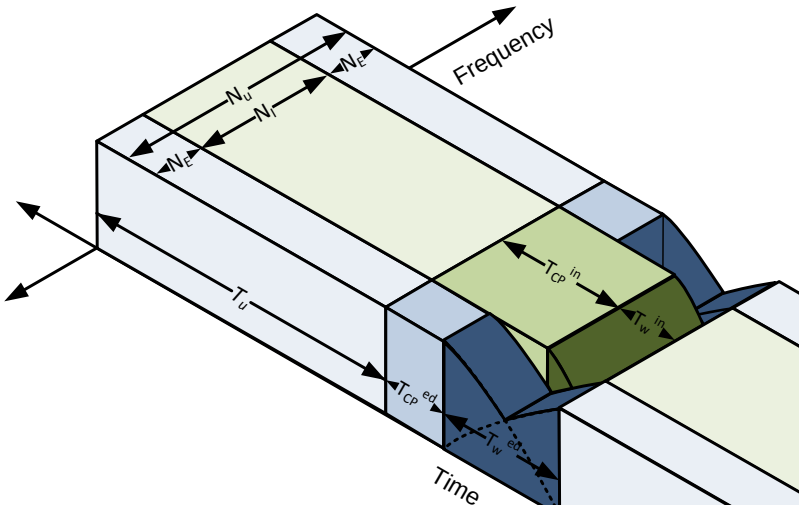

Figure 3.6: Shape of edge windowed OFDM symbol in time and frequency domains.

respectively. In Figure 3.6, the OFDM symbol shape has different CP lengths for each group, which are denoted as T_{CP}^{ed} and T_{CP}^{in}, for the edge and inner groups, respectively. The total OFDM symbol extension is the same for both groups, i.e., $T_w^{ed} + T_{CP}^{ed} = T_w^{in} + T_{CP}^{in}$. While the edge window is considerably longer than the inner window, the effective CP of the inner group is longer than the effective CP of the edge group. This provides more channel delay spread immunity to the inner subcarriers.

This technique can be implemented simply by processing each group separately using separate IFFT, CP and windowing modules for each group. Figure 3.7 shows the basic implementation of edge windowed OFDM model. The orthogonality of the subcarriers is maintained if the multipath delays in the inner and edge subcarriers are shorter than the corresponding CP's. The user allocation block is a scheduling process that allocates users that experience long channel delay spread to inner group with long CP while edge group is reserved for users that endure short channel delay spread with long window. By using such scheduling, the OFDM system is able to support users with long delay spread while providing effective sidelobe suppression [27]. The IFFT block length is the same, N, for all groups and the unused inputs of the IFFT are set to zero.

The computational complexity of OFDM model is doubled compared to basic windowed OFDM, since separated processing is required for each group. Some savings are possible by using pruning methods in the IFFT implementation [28], but we don't consider this possibility in our coarse complexity evaluation. Hence, the added computational complexity of the edge windowing depends on computational complexity of IFFT algorithm that is used in IFFT block. When using the effective

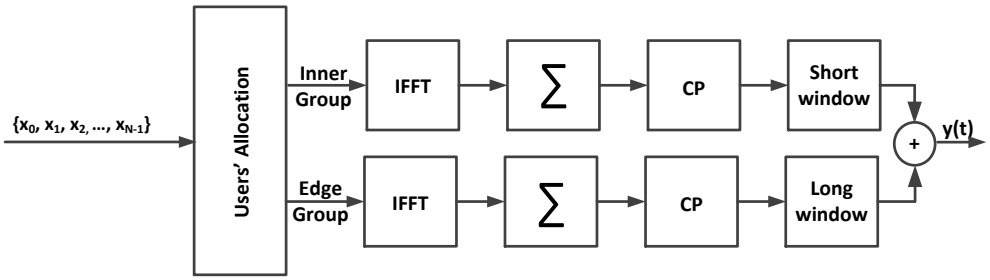

Figure 3.7: Implementation of edge windowing technique.

Split-Radix [29], the added computational complexity compared to basic CP-OFDM, in terms of real multiplications and additions per OFDM symbol, can be formulated as follows:

$$\begin{aligned} \mathcal{C} &= (G-1)\left[N(\log_2 N - 3) + 4\right] + 2\sum_{g=1}^{G} N_w^g \\ \mathcal{A} &= (G-1)\left[3N(\log_2 N - 1) + 5\right] + \sum_{g=1}^{G} N_w^g \end{aligned}, \tag{3.5}$$

where G is the number of subcarriers groups and N_w^g is the window length of gth subcarrier group. Hence, the added computational complexity is proportional to number of groups used for edge windowing.

Properly configured edge windowing has practically as good suppression performance as conventional windowing with the same overall OFDM symbol length. Similar to conventional windowing, edge windowing performance is enhanced rapidly as sidelobes location gets farther away from active subcarriers. Besides, edge windowing with user scheduling can be exploited to increase OFDM system immunity to channel delay spread, especially for users that are located far from the transmitter. Furthermore, edge windowing technique can be combined with partial transmit sequence (PTS) for PAPR mitigation in a computationally effective way. Further details of this combination can be found in [30].

3.2 Cancellation carriers

Basically, the power levels of OFDM sidelobes change instantaneously according to the input symbol values. Therefore, CC technique aims to reduce power of sidelobes at predetermined range by adding properly weighted subcarriers to the deactivated band of OFDM spectrum [7]. Essentially, three major parameters affect the suppression performance. These factors are the number of CC's, width of optimization range and the scheme for calculating the CC weight sequence. The number of CC's and the optimization range are defined according to system requirements and afford-

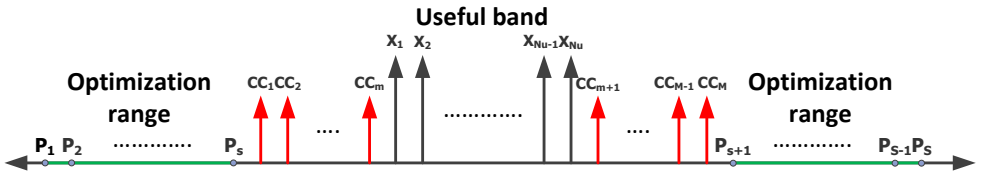

Figure 3.8: Frequency domain representation of OFDM spectrum using CC technique.

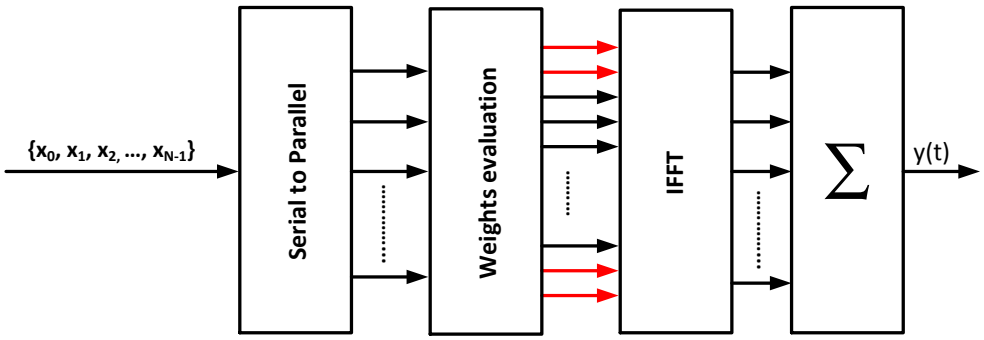

Figure 3.9: Implementation of OFDM model using CC technique.

able computational complexity. Nevertheless, weights evaluation is the main issue in CC technique.

Figure 3.8 shows the frequency representation when CC technique is used. The position of the optimization range is chosen to be as close to the useful band as possible, where the sidelobes power is the highest. Furthermore, the positions of CC's have to be close to the optimization range because the impact of CC is stronger on closer sidelobes.

To find out the required weights, firstly the number of CC's, M, has to be defined. Besides, the location of each CC has to be defined as IFFT input bin k, which is not used as a data subscriber. An unweighted CC is again modeled by a sinc spectrum:

$$CC_k = \text{sinc}\left[T_s\left(f - \frac{k}{T_u}\right)\right]. \tag{3.6}$$

Secondly, the optimization range points, S, has to be defined. The suppression can be applied on all points of the optimization range but the added computational complexity is tremendously increased with the number of optimization points. However, it is sufficient to do the optimization only on the middle between center frequencies of unused subcarriers. Assuming that only subcarrier k is active, those points are located at:

$$f = \frac{\frac{l}{2} + k}{T_u}, \tag{3.7}$$

where l is an odd integer, and the value at that frequency equals:

$$P_l = \frac{(-1)^{\frac{l+3}{2}} cos(l\frac{\pi}{2})}{(1+q)\left(\frac{\pi}{2}l\right)}. \tag{3.8}$$

Here $q = \frac{T_{CP}}{T_u}$, as discussed in Subsection 2.2.2. Consequently, a sidelobe's value of OFDM spectrum at certain location k_s in the optimization range is calculated in the following way:

$$P_s = \sum_{k \in A} \frac{x_k(-1)^{k-k_s+1} h_k}{(1+q)(k-k_s-\frac{1}{2})\pi}, \tag{3.9}$$

where A is the set of active subcarriers and $h_k = \cos(q\pi(k-k_s-0.5))$ is a periodic function changing according to active subcarrier index and the index of the optimization point. Then, the optimization points are collected in column vector $\mathbf{P} = [P_1, P_2, ..., P_S]^T$.

Thirdly, the sidelobe values at the optimization points of CC's are collected. For unweighted CC they are calculated as follows:

$$C_{s,m} = \frac{(-1)^{k_m-k_s+1} h_{s,m}}{(1+q)(k_m-k_s-\frac{1}{2})\pi}. \tag{3.10}$$

where k_m is the CC index within IFFT block. $C_{s,m}$ in Equation (3.10) is an element of matrix $\mathbf{C} = [\mathbf{C}_1, \mathbf{C}_2, ..., \mathbf{C}_M]$ of $S \times M$ elements. Here columns $\mathbf{C}_m = [C_{1,m}, C_{2,m}, ..., C_{S,m}]^T$ represent the points in the optimization range due to one CC.

Then, the unknown weight vector is defined as $\mathbf{G} = [g_1, g_2, ..., g_M]^T$, where g_m is the weight of the mth CC. Finally, the following minimization problem is formulated using the generated matrices:

$$\min_{\mathbf{g}} ||\mathbf{P} + \mathbf{C}\mathbf{g}||^2 \text{ subject to } ||\mathbf{g}||^2 \leq a^2, \tag{3.11}$$

where a^2 is the power limitation of CC's. The problem formulated in (3.11) is a least squares problem with quadratic inequality constraint. The solution of this problem can be found [31] and it is discussed in Appendix A.

Figure 3.9 represents the implementation of OFDM model that utilizes CC technique for sidelobe suppression. The red arrows are the inserted CC's. The weights evaluation block is the only added computational complexity to the OFDM model. However, depending on CC scheme, this block may have a relatively high complexity.

The computational complexity of CC technique is defined by the number of computations needed to solve the weights. This includes (i) calculating the sidelobe value at the optimization point using Equation (3.9) and (ii) finding a solution of

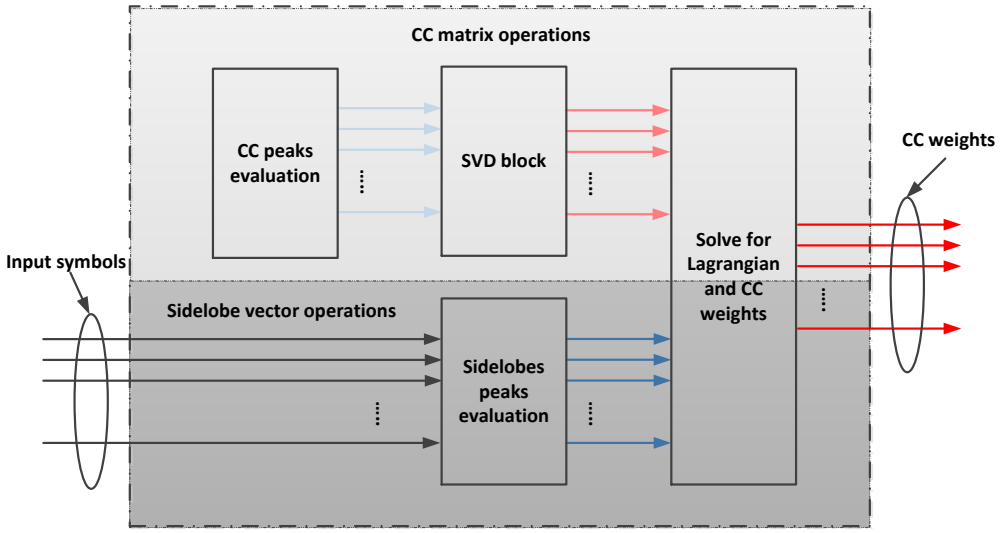

Figure 3.10: Implementation of weights evaluation block.

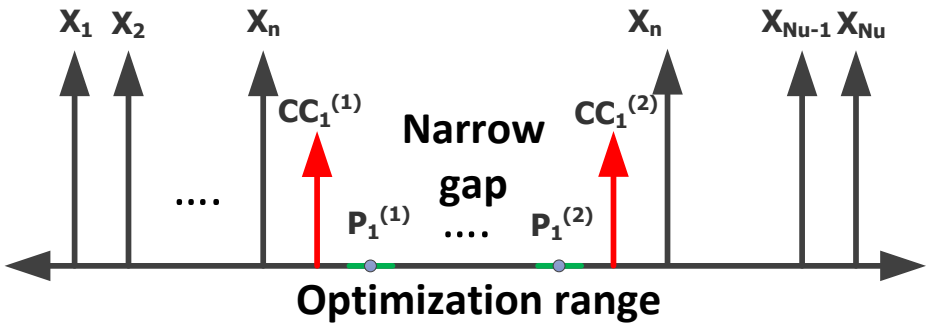

Figure 3.11: Frequency domain implementation of OFDM spectrum using simplified CC technique in a spectrum gap.

the minimization problem (3.11). The values of sidelobes matrix in (3.10) are fixed and need to be calculated only once, or in case of dynamic spectrum use every time after system reconfiguration.

Figure 3.10 shows the implementation of the weights evaluation block mentioned in Figure 3.9. The $\mathbf{C}$ matrix that is resulted from Equation (3.10) is used to compute the singular value decomposition (SVD), which is used to transform the minimization problem (3.11) into simpler form. Therefore, in case of fixed CC configurations, the SVD decomposition can be computed once and fed into Lagrangian and CC solver block which reduces the computational complexity dramatically. Naturally, these calculations have to be repeated after every reconfiguration of the active data subcarriers, CC's and/or optimization range [32]. The computational complexity of CC in the case of dynamic or fixed CC schemes is discussed in Appendix A.

The suppression performance of CC technique is expected to be strong in the optimization range. But, outside the optimization range, the sidelobes power tends to grow towards the sidelobe power of the regular CP-OFDM scheme. However,

increasing the optimization range heavily enlarges the required computational complexity intensively. Therefore, a careful choice of the number of needed CC's and the length of optimization range must be made in order to achieve the required suppression with minimum possible complexity. Performance range limitation of CC motivates the usage of CC especially in non-contiguous OFDM scenarios with narrow gaps, in which case the required optimization range is limited [33]. Nevertheless, the evaluation of CC weights is not restricted to the linear least squares (LLS) problem. In [34], weights are evaluated using genetic algorithm resulting in better sidelobe suppression with complexity increase. Moreover, CC technique increases the PAPR and BER of OFDM system due to due to additional, possibly high-powered subcarriers [35]. On other hand, the CP has a critical impact on CC technique in terms of suppression performance and power consumption [33]. Detailed discussions are presented in Chapter 4 and Chapter 5.

Simplified cancellation carrier

The suppression performance of CC technique is high in the optimization range. But the relatively high computational complexity of CC is still a major obstacle. Hence, there is a need for reducing the computational complexity of CC technique in order to achieve an acceptable suppression with the lowest possible computational complexity. We focus on reducing the sidelobe levels assuming that just one or two CC's are inserted at each edge to optimize the next one or two sidelobes. These cases are referred to as simplified 1 cancellation carrier and 1 optimization point (1CC) and simplified 2 cancellation carriers and 2 optimization points (2CC) schemes. Each CC weight (1CC) or pair of weights (2CC) is evaluated independently of the others [26]. Figure 3.11 shows the proposed positions of each CC and the optimization range that are optimized separately, for 1CC scheme.

In simplified CC, the implementation of weight evaluation block is significantly reduced because of the nonlinear relation between the number of CC's and number of optimization point with computational complexity.

The suppression performance of the simplified CC is close to suppression provided by the regular CC with the same configuration. This is because the CC's located far from optimization range have weak effect

3.3 Polynomial cancellation coding

PCC is a technique that is used to reduce OFDM sensitivity to frequency errors [36] and phase errors. The benefits of PCC technique includes the spectral enhancement, i.e, reducing sidelobes powers significantly. PCC divides the useful part of the IFFT block into identical groups. Each group contains m subcarriers representing one

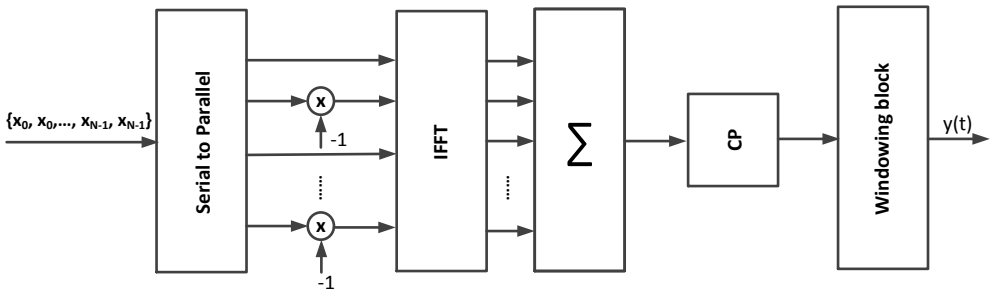

Figure 3.12: Implementation of PCC-OFDM for groups of two subcarriers.

data symbol x_k in such a way that each subcarrier in the group is multiplied by the coefficients of the following polynomial:

$$(1-x)^{m-1}. \tag{3.12}$$

The commonly used number of subcarrier per group is $P = 2$ in which case the coefficients of the Expression (3.12) are defined as $a_0 = 1$ and $a_1 = -1$. In general, each subcarrier is represented in frequency domain as follows:

$$Y_{kP+p}(f) = T_u a_p \text{sinc}\left[fT_u - k - p\right] \text{ for } p = 0, 1, ...P-1. \tag{3.13}$$

For $P = 2$, the subcarrier group spectrum becomes:

$$Y_{2k}(f) - Y_{2k+1}(f) = x_k \frac{T_u \text{sinc}\left[T_u f - 2k\right]}{T_u f - 2k - 1}. \tag{3.14}$$

The resulting fraction in Equation (3.14) reduces the sidelobes of the OFDM spectrum [9].

The implementation of PCC technique for $P = 2$ is depicted in Figure 3.12. There is no additional computational complexity, however the scheme has the major drawback of reduced spectral efficiency by the factor of two.

The resulting suppression performance of PCC is high in subcarriers far from the used subcarriers, similar to time domain windowing case. In fact, in time domain PCC can be represented as OFDM symbols multiplied by a complex window.

3.4 Subcarrier weighting

Each subcarrier in OFDM spectrum is weighted by IFFT input data symbol x_k, which varies instantly according to sent information. Different combinations of the subcarriers weights yield different spectral shapes at sidelobes. The subcarrier weighing (SW) technique aims to multiply the subcarriers by specific weights in such a way that the sidelobes powers are reduced [8]. The primary task in SW is the

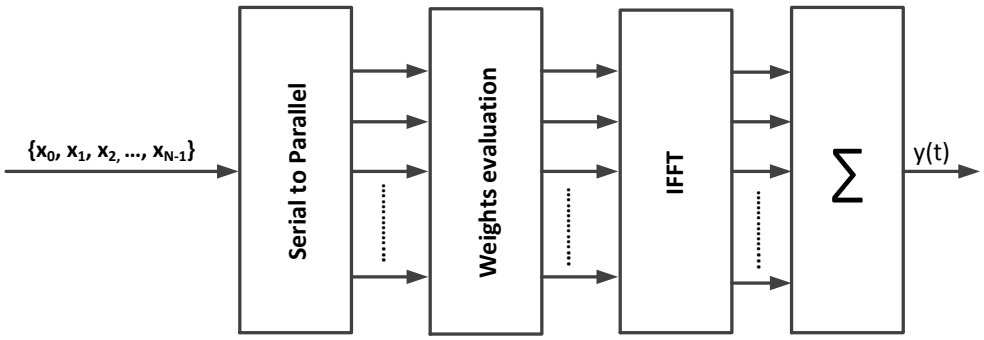

Figure 3.13: Implementation of SW OFDM.

subcarrier weight optimization. Two parameters are needed to be defined for the optimization: (i) range of the subcarrier weights, (ii) optimization range, i.e., the set of sidelobes whose energies are used in the minimization. The importance of the weight range is that that it guarantees certain amount of power for each subcarrier symbol, while fixing the overall transmission power level.

Equation (3.10) can be used for determining the PSD peaks of each subcarrier within the optimization range. The sidelobes values in between two subcarriers are collected in matrix $\mathbf{P}$ of size $M \times N_u$, where M is the number of sidelobes in the optimization range. The positive, real subcarriers weights are assigned in the column vector $\mathbf{g} = [g_0, g_1, ..., g_{N_u-1}]^T$. Then the following minimization problem can be formulated:

$$\min_{\mathbf{g}} ||\mathbf{Pg}||^2 \text{ subject to } g_{min} \leq g_n \leq g_{max} \text{ and } ||\mathbf{X}||^2 = ||\bar{\mathbf{X}}||^2, \tag{3.15}$$

where $\mathbf{X} = [x_0, x_1, ..., x_{N_u-1}]^T$ is the data symbol vector and $\bar{\mathbf{X}} = [g_0 x_0, g_1 x_1, ..., g_{N_u-1} x_{N_u-1}]$ is weighted symbol vector. Problem (3.15) is a nonlinear optimization problem with quadratic equality and linear inequality. The solution of this problem can be found in [37].

SW implementation is illustrated in Figure 3.13 where the evaluation block produces the weighted subcarriers that are fed to IFFT. The computational complexity of SW is high compared to CC technique considering that the used input matrix has a high number N_u rows and the non-linearity of the optimization problem.

In the SW method, no side information is transmitted about the subcarrier weights. Instead, the idea is that the weight range is small enough so that the random variations in the subcarrier symbol values do not essentially degrade the detection performance. This works well for low order constellations, BPSK or QPSK, or PSK type modulations. In those cases, the weighting does not affect the decision regions of the receiver, and just the variations of the subcarrier symbol powers affect the BER performance. However, for high order QAM constellations the weight range should be small and the sidelobe suppression performance would be quite limited.

In the same way as in CC, the sidelobe suppression performance of SW is high in the optimization range, whilst the performance outside the optimization range is weaker and approaches OFDM at far sidelobes. Hence, SW usage at narrow gaps is expected to be more efficient than in the guard bands of the overall spectrum.

4. SUPPRESSION PERFORMANCE IN 5 MHZ 3GPP LTE CASE STUDY

In this chapter, the sidelobe suppression of the presented techniques is investigated at different cases and scenarios. The suppression performance is tested in the practical case study using 5 MHz 3GPP LTE parameters and considering both contiguous and non-contiguous scenarios.

The first section introduces the main parameters of 3GPP LTE 5 MHz model which are necessary for the configuration of the applied techniques. Besides, the contiguous and non-contiguous scenarios are described carefully. The second section illustrates the suppression performance of time domain windowing and edge windowing technique. In the third section, the simplified CC technique is elaborated. Then the effect of CP length on the performance of the CC technique is examined justifying the need for limitation. The fourth section shows the suppression performance of PCC. The effect of CP on PCC is depicted. The fifth section discusses the SW suppression performance with CP effect. The sixth section describes the edge windowing and simplified CC combination. Then, it represents the suppression performance of the technique.

4.1 5 MHz 3GPP LTE model

LTE stands for Long Term Evolution that is a wireless communication standard for high-speed mobile cellular networks. The standard was developed by 3rd Generation Partnership Project (3GPP) and it was defined in its Release 8 document series. The fundamental goal of LTE standard is to increase the speed of wireless transmission, reduce connection latency and migrate the network to all IP-flat network.

From spectral aspects, LTE standard aims to improve the spectral efficiency of the mobile system through various solutions. Firstly, LTE employs OFDM scheme. Secondly, LTE standard allows mobile operators to run their systems over a variety of bandwidths, e.g., 1.4, 3, 5, 10, 15 and 20 MHz. This gives the flexibility to run the LTE standard in various wireless environments. Thirdly, the LTE allows base stations and mobiles to operate over a large number of frequency bands. This permits the operators to use the system according to the regulations of each country. Therefore, LTE standard has a great potential to to be exploited also in challenging spectrum access scenarios, like cognitive radio.

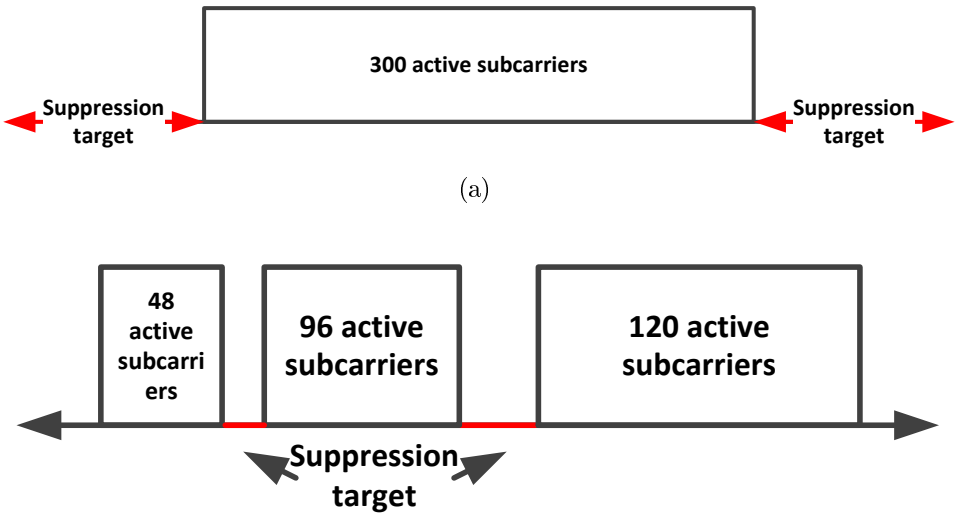

Figure 4.1: 5 MHz LTE configurations with (a) contiguous and (b) non-contiguous spectrum use. The target frequency slots for sidelobe suppression are indicated.

Basically, LTE divides time domain into 0.5 ms pieces which are called slots. The number of OFDM symbols contained in each slot is dependent on the of CP mode used in LTE. LTE model supports two CP modes: (i) normal CP mode that divides the slot into 7 OFDM symbols and (ii) extended CP mode that divides the slot into 6 OFDM symbols. The useful duration of OFDM symbol is $T_u = 66.7$ μs for both normal and extended modes. This results in frequency spacing between subcarriers of 15 kHz. The duration of CP is 4.7 μs in normal mode, and it is 16.7 μs in extended mode. However, the duration of the first symbol in the slot is 5.2 μs in the normal CP mode. Regarding the bandwidth, the chosen bandwidth in this study is 5 MHz which is a common case in wireless communications. The 5 MHz LTE model is implemented using 512 IFFT points. Hence, the CP length is defined as $N_{CP} = 36$ and $N_{CP} = 128$ in the normal CP and extended CP modes, respectively. The sampling frequency is $\frac{1}{T} = 7.68$ MHz. The useful band consists of 30 resource blocks (RB) and each RB contains 12 subcarriers. Hence, the number of useful subcarriers is $N_u = 300$ and they occupy 4.5 MHz of the spectrum. Consequently, the used guard band is 0.25 MHz on both sides of the useful spectrum.

In the simulations, 5 MHz LTE configuration is used with different CP modes, so each technique is tested with different CP lengths. An exception to LTE standard is considered: the zero prefix (ZP) mode, which from the sidelobe suppression point of views corresponds to the CP case when the CP length approaches zero. The simulations were run over 100,000 symbols using BPSK modulation.

Figure 4.1 demonstrates the sidelobe suppression target frequencies in the contiguous and non-contiguous scenarios. In Figure 4.1(a), the suppression targets are

the guard bands of LTE standard. Both guard bands contain 16 sidelobes in the chosen scenario. Figure 4.1(b) illustrates the number of gaps and their locations in the used non-contiguous scenario containing two gaps of different sizes, 1 resource block (1RB) and 2 resource blocks (2RB). The presented non-contiguous scenario is a typical case where the nominal frequency band is not completely available. Nevertheless, the numerical configuration of each technique is clarified in each section.

4.2 Time domain windowing methods

In the 5 MHz LTE scenario, the extended CP mode provides sufficient resources for the time required for time windowing methods. The choice of window length is based on reaching the maximum possible roll-off while keeping the minimum required CP in the standard. In conventional time domain windowing, the following parameters are used:

- CP length: $N_{cp} = 36$ samples.
- Window transition length: $N_w = 92$ samples.

This results into a roll-off factor of $\alpha = 0.1437$. Regarding edge windowing, more parameters have to be defined. The edge group contains two RB's around the edges, while the inner group contains the remaining subcarriers. The number of edge subcarriers is chosen to allow sufficient suppression while providing longer CP for more users. Accordingly, the following parameters are used:

- Size of edge subcarriers group: 2RB.
- Edge window transition length: $N_w^{ed} = 92$.
- CP length in edge subcarriers: $N_{cp}^{ed} = 36$.
- Inner window transition length: $N_w^{in} = 32$.
- CP length in inner subcarriers: $N_{cp}^{in} = 96$.

Hence, the used roll-off factors are $\alpha^{ed} = 0.1437$ and $\alpha^{in} = 0.05$ for edge and inner groups, respectively.

The suppression performance of both windowing methods in the contiguous scenario is depicted in Figure 4.2 where the data cursors illustrate the power at 0.25 MHz away from useful band. Both windowing methods show a relatively high suppression performance compared to CP-OFDM with power levels of 42.75 dB and 39.68 dB less than CP-OFDM at the same points. Generally, the effect of windowing methods is weak on sidelobes close to the edge. The first and second sidelobes power are only 2 dB and about 3 dB lower than CP-OFDM sidelobes, respectively,

for both techniques. The suppression performance increases as sidelobes get far from useful band edges. Generally, the conventional windowing performs better than edge windowing because of the effect of inner subcarriers, since the inner group has shorter window length.

Similarly, both windowing methods were tested in the non-contiguous scenario. Figure 4.3 shows that the power levels of the middle sidelobes are at -37.97 dB and -57.39 dB in the 1RB gap and 2RB gap, respectively, when conventional windowing is used. The resulting power in the middle sidelobes using edge windowing are -24.14 dB and -34.42 dB in 1RB and 2RB, respectively. This reveals a big difference in the performance, which is explained in Figure 4.4. The inner group leaks strong sidelobe power to the gaps. Therefore, the edge windowing performance follows the inner subcarrier performance in the gaps.

Therefore, improvement is required for edge windowing to overcome the suppression performance limitations. Simply, adding the gap edges to the edge group reduces the power leakage which results from the inner group. This improvement doesn't require any extra computational complexity. But scheduling is required to adapt to the dynamic edging method. In Figure 4.5, the PSDs of CP-OFDM, conventional windowing and dynamic edge windowing are depicted. The resulting suppression of dynamic edge windowing is approximately identical to that of the conventional windowing. Figure 4.6 shows that the suppression performance of dynamic windowing is practically equal to the conventional windowing in the first gap, see Figure 4.6(a). While in Figure 4.6(b), the suppression performance of dynamic edge windowing is 0.73 dB less than conventional windowing. Figure 4.7 shows that the inner subcarriers sidelobes are kept lower than those of the edge subcarriers. Consequently, the suppression is enhanced, leading to practically the same performance as conventional windowing.

The resulting performance of dynamic windowing is very close to conventional windowing. Nevertheless, both techniques have a major drawback that the suppression is relatively low in the sidelobes close to the gap edges.

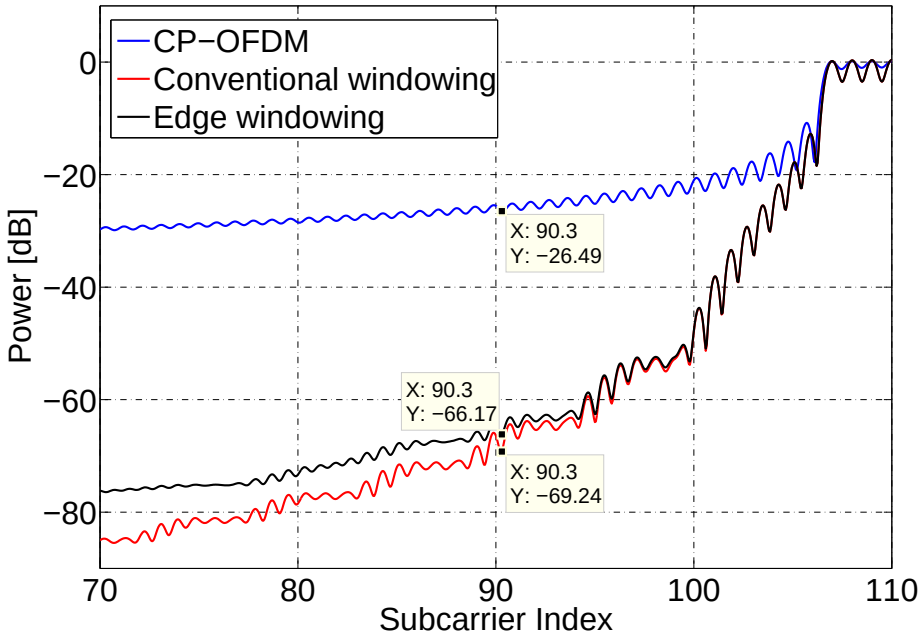

Figure 4.2: PSD performance of conventional and edge windowing performance in contrast to CP-OFDM in the contiguous scenario.

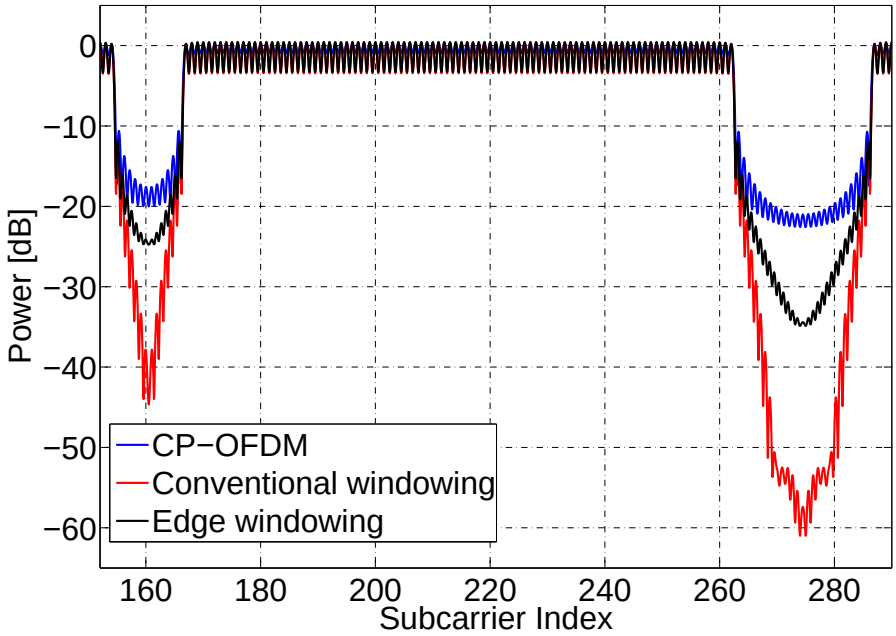

Figure 4.3: PSD performance of conventional and edge windowing performance in contrast to CP-OFDM in the non-contiguous scenario.

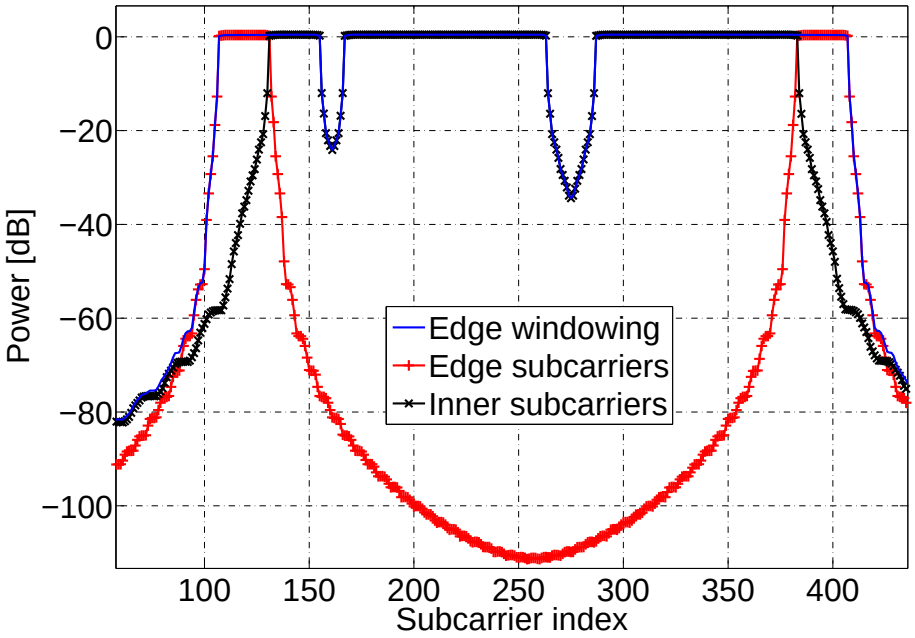

Figure 4.4: Detailed PSD of edge windowing showing the behavior of edge group and inner group in the non-contiguous scenario.

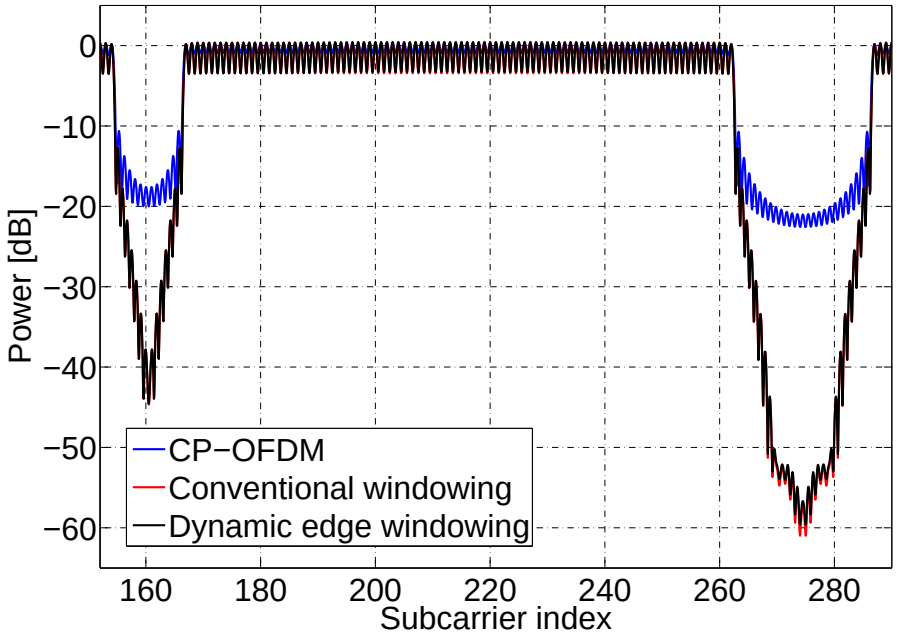

Figure 4.5: PSD performance of conventional and dynamic edge windowing performance in contrast to CP-OFDM in the non-contiguous scenario.

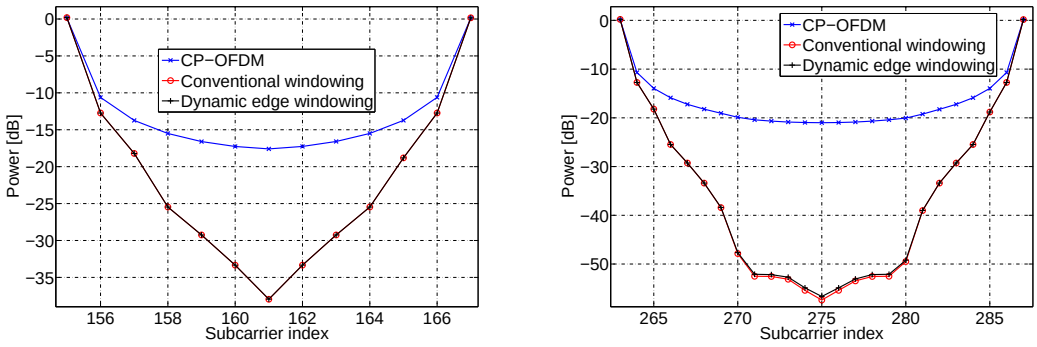

(a) 1RB gap. (b) 2RB gap.

Figure 4.6: Zoomed PSD peak envelope of the two gaps in the non-contiguous scenario.

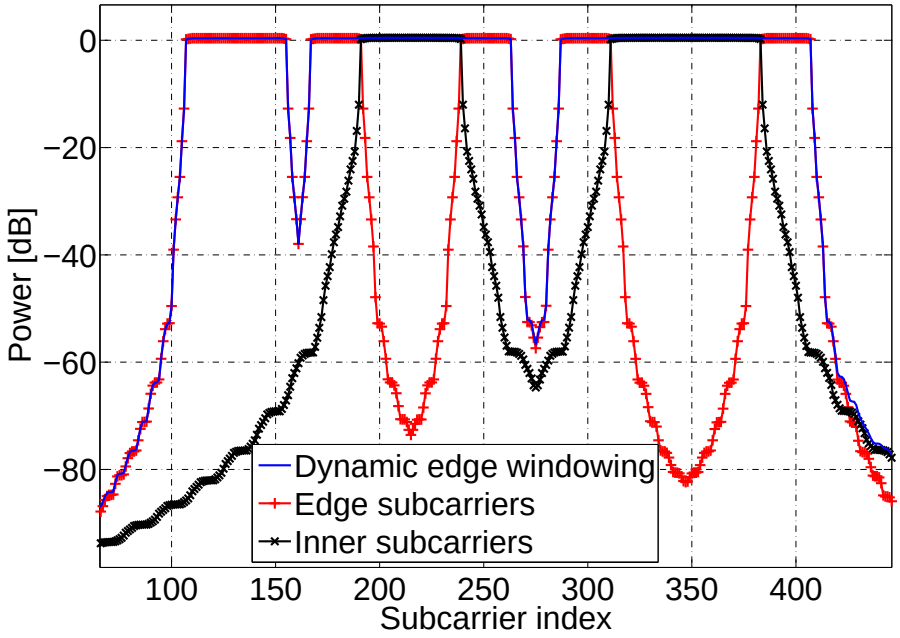

Figure 4.7: Detailed PSD of dynamic edge windowing showing the behavior of edge group and inner group in the non-contiguous scenario.

4.3 Cancellation carrier methods

The CC-methods are tested in the ZP, normal CP and extended CP modes to consider the effect of different CP lengths on the suppression performance of CC. Basically, the CC technique is considered as fixed in the contiguous scenario and dynamic in the non-contiguous scenario. Furthermore, the simulations use different CC schemes, e.g., simplified and conventional, limited and unlimited, 1CC and 2CC. The configurations of the tested CC schemes in the contiguous scenario are:

- Indexes of 1CC: 106 and 407.

- Indexes of 2CC: 105, 106, 407 and 408.
- Indexes of one optimization point: 104.5 and 408.5.
- Indexes of two optimization points: 102.5, 103.5, 409.5 and 410.5.

For the non-contiguous 5 MHz LTE scenario, the used configurations are:

- Indexes of 1CC: 155, 166, 263 and 286.
- Indexes of 2CC: 155, 156, 165, 166, 263, 264, 285 and 286.
- Indexes of one optimization point: 156.5, 164.5, 264.5 and 284.5.
- Indexes of two optimization points: 157.5, 158.5, 162.5, 163.5, 265.5, 266.5, 282.5 and 283.5.

4.3.1 Simplified CC justification

In first test, it is important to evaluate the impact of CC's on far optimization points in the contiguous scenario. A suitable scheme is to use the conventional 1CC without power limitation. Figure 4.8(a) shows the PSD of OFDM with one CC at one edge. Clearly, the power leaked from the cancellation subcarrier is -59.65 dB on the optimization point on the other edge. This is considered as a very weak effect on that point. A zoomed PSD at the guard band, Figure 4.8(b), shows that identical suppression performance of conventional and simplified 1CC. As a result, simplified CC technique is more feasible considering its reduced computational complexity.

In the second test, the impact of CC on the optimization point located at other gap edges is evaluated in the non-contiguous scenario. Therefore, 1CC without power limitation is applied in Figure 4.9. In Figure 4.9(a), the unweighted subcarrier leaks -29.5 dB to the optimization point at 156.5. The leaked power is relatively high compared to the previous test because the cancellation subcarrier is 10 subcarriers away from the considered optimization point. Meanwhile, the effect of the shown 1CC is weak on optimization points located at 264.5 and 284.5 in the other gap. Figure 4.9(b) shows that simplified 1CC has a slight reduction in suppression performance in the gaps. The suppression performance of simplified 1CC is about 3.7 dB lower that of the conventional 1CC.

Generally, the suppression performance of the CC technique is strong in the optimization range if the optimization range is close to the CC's. However, if the optimization point is not close to CC, the resulting suppression will be weak or more power have to be applied on CC's. In simplified CC scheme, the previous results match conventional CC; however simplified CC is much less complicated than conventional CC. Therefore, conventional 1CC is skipped later on this document.

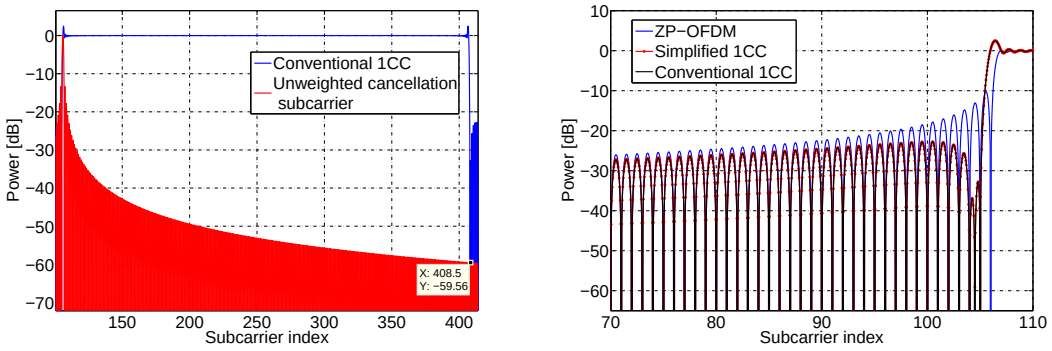

(a) (b)

Figure 4.8: (a) Effect of unweighted cancellation subcarrier on far optimization point. (b) Zoomed PSD on the guard band.

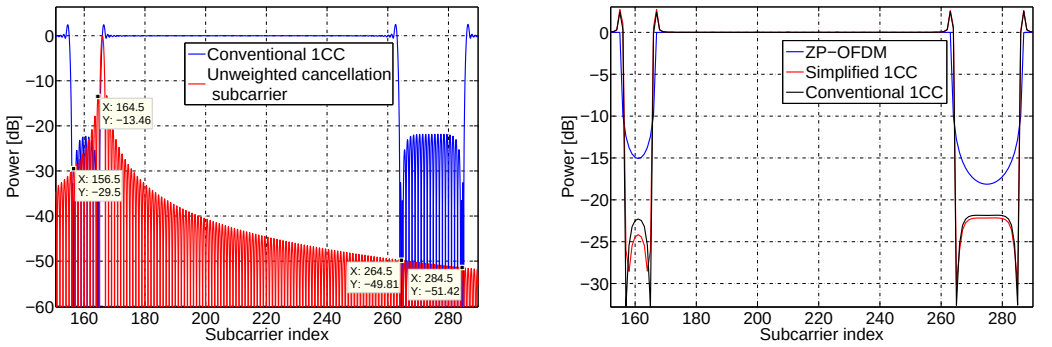

(a) (b)

Figure 4.9: (a) Effect of unweighted cancellation subcarrier on far optimization point. (b) Zoomed PSD envelope on the gaps.

- CC schemes in the normal CP mode.
- Simplified 1CC scheme in the extended CP mode.

The shifted normal CP mode is not considered because of the high power required and extra complexity added to compute the shifted optimization points as well as weak performance.

4.3.2 CP effect

In the third test, the impact of CP length on CC performance in the contiguous scenario is investigated. Schemes of simplified 1CC, simplified 2CC and conventional 2CC are applied without power limitation. Figure 4.10 shows the suppression performance of different CC configurations for the ZP, normal CP and extended CP modes. The simplified 1CC scheme suppresses the first sidelobe to -37 dB, while simplified 2CC and conventional 2CC provides -52 dB and -56 dB levels, respectively. Regarding the normal CP mode, Figure 4.10(b) demonstrates that CC

techniques cause deep notches at the optimization points. However, there is an overall increment in sidelobe power levels. One solution to that problem is to shift the optimization point at 102.5 and 410.5 to 103 and 410, respectively. In Figure 4.10(c), shifting reduces the distance between two consecutive optimization points resulting in a considerable enhancement of 2CC techniques that reaches -30 dB in the optimization range. In Figure 4.10(d), 2CC schemes provide strong suppression in the optimization range. Nevertheless, while simplified simplified 1CC technique causes deep notch in the optimization point, the suppression effect is negligible outside the optimization point.

In the fourth test, CC techniques is applied on CP OFDM with different CP lengths in the non-contiguous scenario. In Figure 4.11, CC configurations show the best suppression performance to the ZP mode, in comparison with the extended or normal CP modes. In Figure 4.11(a), the ZP mode is applied. The simplified 2CC performs worse than simplified 1CC in the 1RB gap because of the small size of the gap. The second optimization point on one edge of 1RB gap is 6 sidelobes away form second CC on the other edge. This explains the inefficient performance of simplified 2CC in 1RB gap. In Figure 4.11(b), simplified 1CC shows a weak reduction on sidelobe in the gaps. The 2CC schemes produce higher sidelobes than sidelobes of CP-OFDM. The effect of 2CC schemes appears as deep notches at the optimization points. Therefore, shits have to be done on optimization points of 2CC schemes that are located at 158.5, 162.5, 266.5 and 282.5 to 158, 163, 266, 283 and 283.5, respectively. The suppression performance of shifted 2CC schemes is notably enhanced as demonstrated in Figure 4.11(c). Regarding the extended CP mode in Figure 4.11(d), the 2CC methods reduces the sidelobe in the optimization range significantly. However, simplified 1CC configuration increases the power of the sidelobes in the gaps except for the deep notches located at the optimization points.

The zoomed Figure 4.12 illustrates the suppression performance of simplified 1CC scheme that performs the best in the ZP mode reaching less than -25 dB and -30 dB levels in the 1RB and 2RB gaps, respectively. However, the suppression performance is reduced dramatically in the normal and extended CP modes. Regarding the simplified 2CC scheme that is shown in Figure 4.13(a), the suppression performance in the 1RB gap is the best in the extended CP mode reaching less than -30 dB power level. However, when using the normal CP mode, the suppression performance is greatly reduced. The shifting of the optimization points enhances the suppression at normal mode slightly. In general, the simplified 2CC method on 1RB gap has a weak suppression performance because the optimization points are close to the next CC on other edge. Figure 4.13(b) shows the suppression performance of simplified 2CC in the 2RB gap. The best suppression is reached in the ZP mode, while the

suppression in the normal CP mode is lower than CP-OFDM performance. Shifting the optimization points results in slight suppression enhancement in the normal CP mode, reaching -22 dB level. Figure 4.14 illustrates the suppression performance of the conventional 2CC scheme. Generally, the suppression performance of the conventional method is similar to the simplified 2CC method except for the ZP mode in the 1RB gap. In Figure 4.14(a), the suppression performance of conventional 2CC is less than -50 dB in the optimization point. However, the suppression is ineffective in the normal CP mode. Shifting causes enhancement in the suppression to about -28 dB. Regarding the extended CP mode, the suppression is around -30 dB. Figure 4.14(b) depicts the suppression performance of conventional 2CC method in the 2RB gap. The best performance is achieve in the ZP mode that it is lower than -50 dB in the optimization range. The suppression performance is insufficient in the normal CP mode. However, shifting enhances the suppression to the level of -27 dB in the optimization range. The suppression performance in the extended CP mode is around -30 dB, which is acceptable.

The previous two tests reveal the general behavior of the CC technique in different schemes, scenarios and CP modes. Generally, the direct conclusion is that CP has a destructive impact on the performance of the CC technique. The reduction in suppression performance is not related to the length of the CP, but it is related to the ratio between the length of CP and the useful part of the OFDM symbol, q, see Equation (2.20). Generally, the most effective part of CC is the peak of the first ripple. However, the shifts caused by the CP result in reduction of the CC performance. The non-orthogonality causes additional cosine components to appear at the normal sidelobe center. Consequently, the number of cosine components depends on the ratio, as discussed in Subsection 2.2.2. This explains why the performance is better in the extended mode as the cosine components are few. Moreover, the increment of the cosine components requires more power to perform the suppression at the optimization range, reducing the effect of CC's outside the optimization range. In the normal CP mode, the sidelobes outside the optimization range get higher than CP-OFDM. Regarding the simplified 1CC scheme, the suppression performs fine in the ZP mode. But, the suppression performance is insufficient in the normal and extended CP modes. Power limitation may become necessary if CC powers become high compared to active subcarriers, i.e., Figure 4.11. However, the power limitation value have to be chosen carefully as the suppression performance is affected. Later on, following schemes are skipped due to insufficient performance: (i) CC method in the normal CP mode. (ii) Simplified 1CC scheme in the extended CP mode. The shifted 2CC in the normal CP mode is not considered because of the high power required and extra complexity added to compute the shifted optimization points and as well as weak performance.

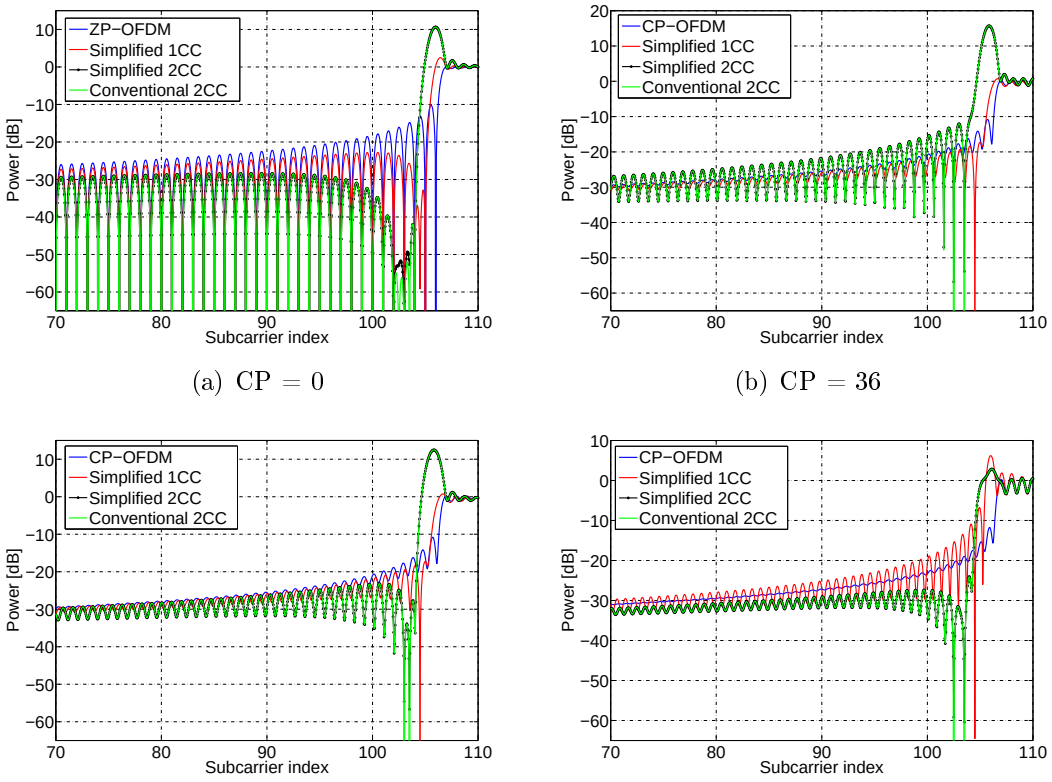

(a) CP = 0

(b) CP = 36

(c) CP = 36 with shifted optimization points

(d) CP = 128

Figure 4.10: Zoomed PSD on the guard band for different CP lengths in the contiguous scenario.

4.3.3 Limited CC scheme

Nevertheless, the average power level of the CC's is high as shown in Figure 4.11. Therefore high peaks are more probable to be generated so that the PAPR is increased. Moreover power consumption in OFDM system affects the BER. Hence it is important to apply the power limitation. PAPR, power consumption and BER are discussed in Sections 5.2, 5.3 and 5.4, respectively. The fifth scenario applies 16 dB power limitation on 2CC schemes in the ZP mode and the extended CP mode. The limitation is not applied on the simplified 1CC scheme due to small average power required in different scenarios. Regarding the contiguous case, the power requirements of 2CC schemes are small; therefore, limitation is neglected in the contiguous scenario.

Figure 4.15 shows a reduction in the suppression performance compared to the unlimited schemes. Nevertheless, the limited simplified 2CC scheme shows higher sidelobes power outside the optimization range in the 2RB gap. Fortunately, the performance of limited simplified 2CC scheme in 1RB gap is enhanced. Figure 4.16 shows that the performance of limited and unlimited cases match in the extended CP mode matches because the power required in unlimited case is close to 16 dB.

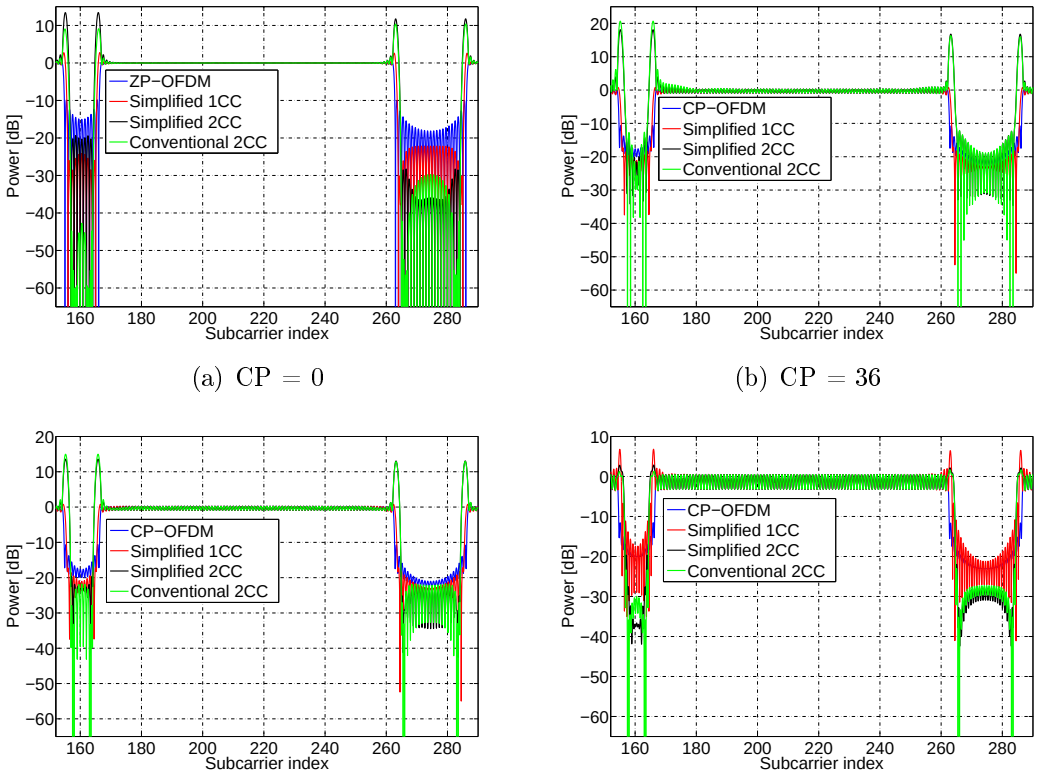

(a) CP = 0

(b) CP = 36

(c) CP = 36 with shifted optimization points

(d) CP = 128

Figure 4.11: Zoomed PSD on the gaps for different CP lengths in the non-contiguous scenario.

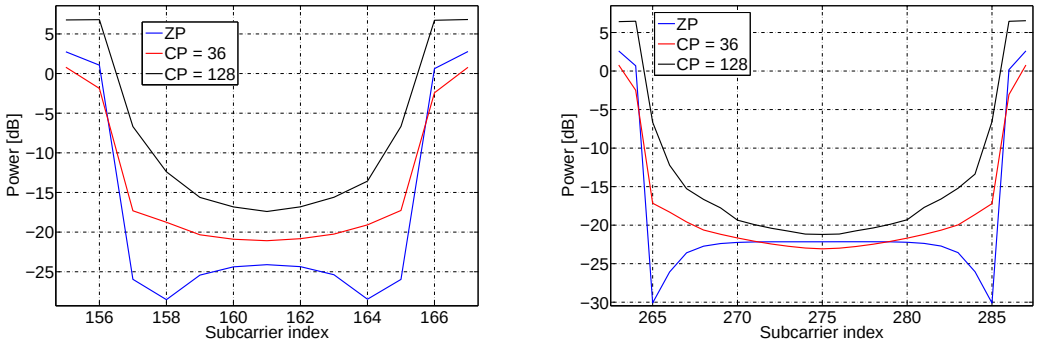

(a) 1RB gap.

(b) 2RB gap.

Figure 4.12: Zoomed PSD peak envelope of the two gaps for the simplified 1CC method using different CP lengths.

Basically, the power limitation reduces the suppression performance of CC technique. Nevertheless, limited simplified 2CC scheme shows better suppression than its unlimited scheme in 1RB gap. The reason is that the sidelobes in limited scheme are accumulated to reduce the sidelobes in the gaps. In the extended CP mode, the performance of unlimited schemes are close to unlimited schemes, because the power requirements in unlimited case is close to the power limitation. Therefore, it is not

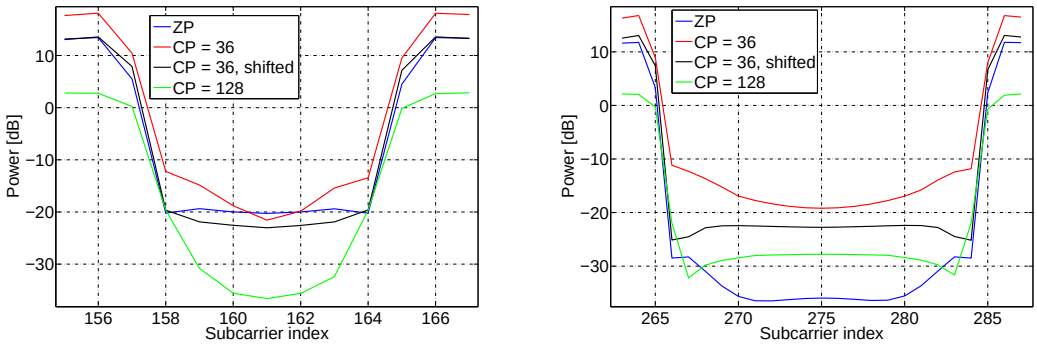

(a) 1RB gap. (b) 2RB gap.

Figure 4.13: Zoomed PSD peak envelope of the two gaps for the simplified 2CC method using different CP lengths.

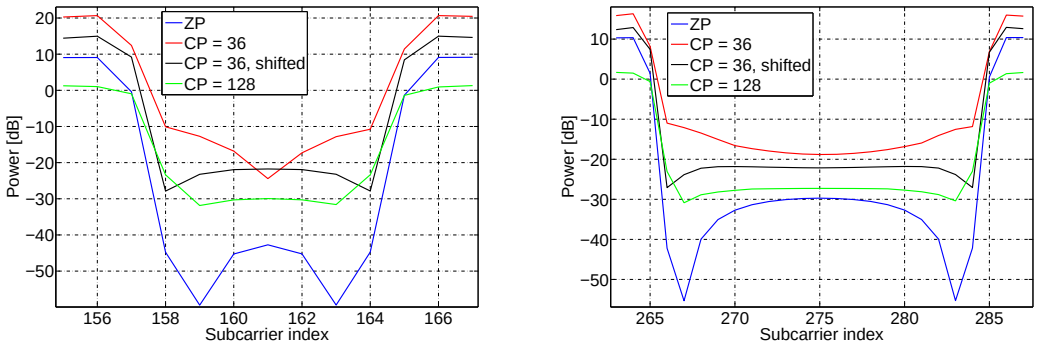

(a) 1RB gap. (b) 2RB gap.

Figure 4.14: Zoomed PSD peak envelope of the two gaps for the conventional 2CC method using different CP lengths.

necessary to use limitation in that mode considering the extra complexity required for limitation, check Section 5.3. Consequently, limitation scheme in extended mode is skipped later on in this document.

Generally, the mentioned conclusions of the need of power limitation in different CP modes is applied only for the above mentioned non-contiguous scenario. However, the requirement for limitation is necessary in general non-contiguous cases for different locations and widths of the spectral gaps, or for other constellations than BPSK.

4.4 Polynomial cancellation coding

In PCC, the degree of polynomial used in the simulations is 2 to keep the spectral efficiency as high as possible. Then, the contiguous and non-contiguous scenarios are applied with different CP modes.

The first scenario of the contiguous 5 MHz LTE is shown in Figure 4.17. The resulting PSD of PCC performs the best in the ZP mode where the first sidelobe is

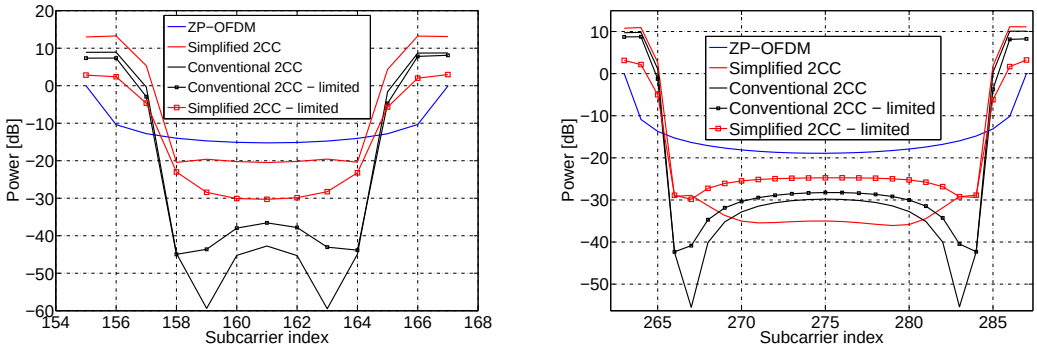

(a) 1RB gap. (b) 2RB gap.

Figure 4.15: Zoomed PSD peak envelope of the two gaps for limited 2CC methods using the ZP mode.

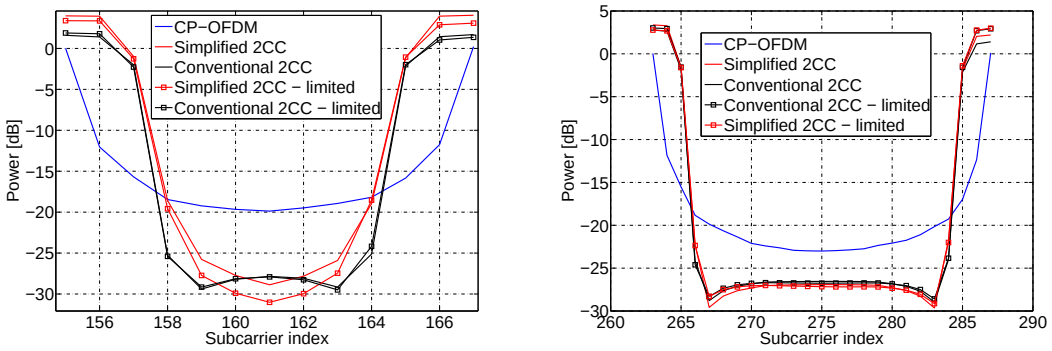

(a) 1RB gap. (b) 2RB gap.

Figure 4.16: Zoomed PSD peak envelope of the two gaps for limited 2CC methods using the extended CP mode.

below -20 dB. The usage of CP reduces the suppression performance of PCC. Anyway, the suppression in both CP modes is sufficient knowing that the first sidelobe is reduced by 6 dB and 10 dB in the extended and normal CP modes, respectively.

The non-contiguous scenario is depicted in Figure 4.18. The suppression performance of PCC in the ZP mode reaches -38.26 dB and -47.14 dB for 1RB gap and 2RB gap, respectively. Again, the use of CP causes a reduction in the suppression performance of the PCC technique. The sidelobe peak power in normal mode is -33.75 dB and -37.1 dB at 1RB gap and 2RB gap, respectively. In the extended CP mode, the corresponding values are -24.99 dB and -28.31 dB.

In conclusions, PCC has a relatively high suppression performance both in the guard bands and in the spectral gaps. However, longer CPs cause a considerable reduction in suppression performance of PCC.

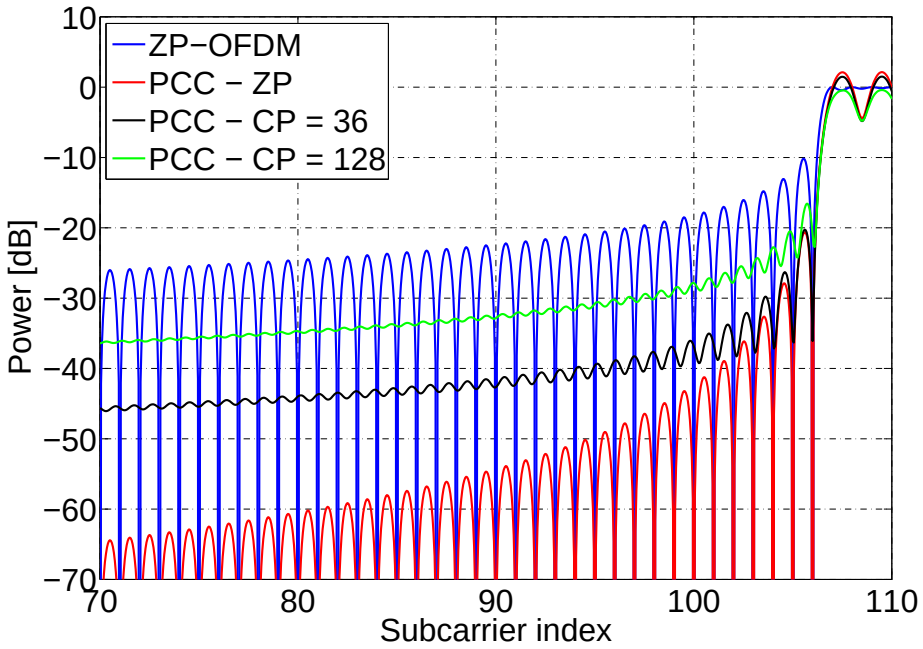

Figure 4.17: Zoomed PSD on the guard band for PCC in the contiguous scenario with different CP modes.

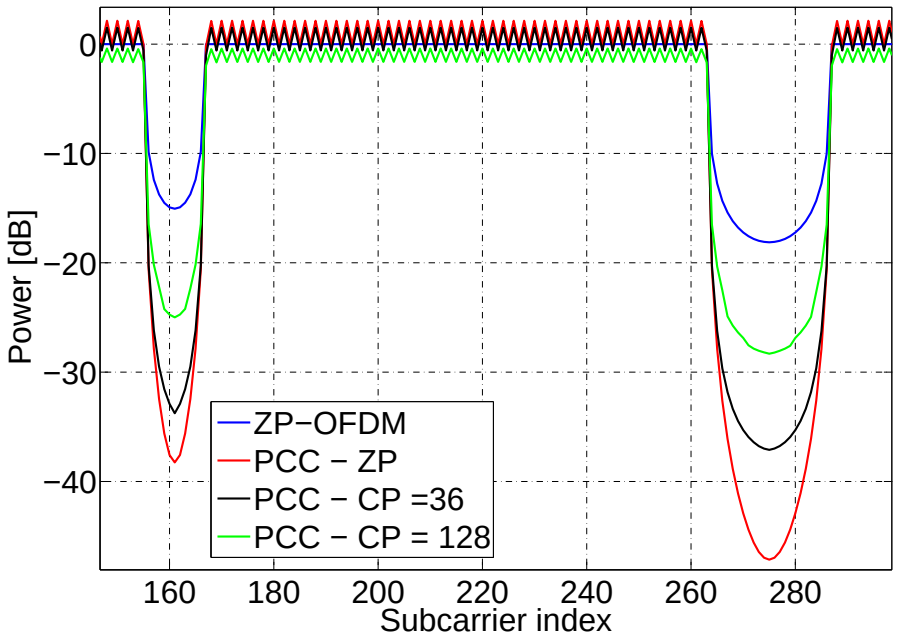

Figure 4.18: Zoomed peak envelope of PSD on the gaps for PCC in the non-contiguous scenario with different CP modes.

4.5 Subcarrier weighting

In the contiguous scenario, the optimization range for the SW method covers the first 5 sidelobes in the guard band. Regarding the non-contiguous scenario, the

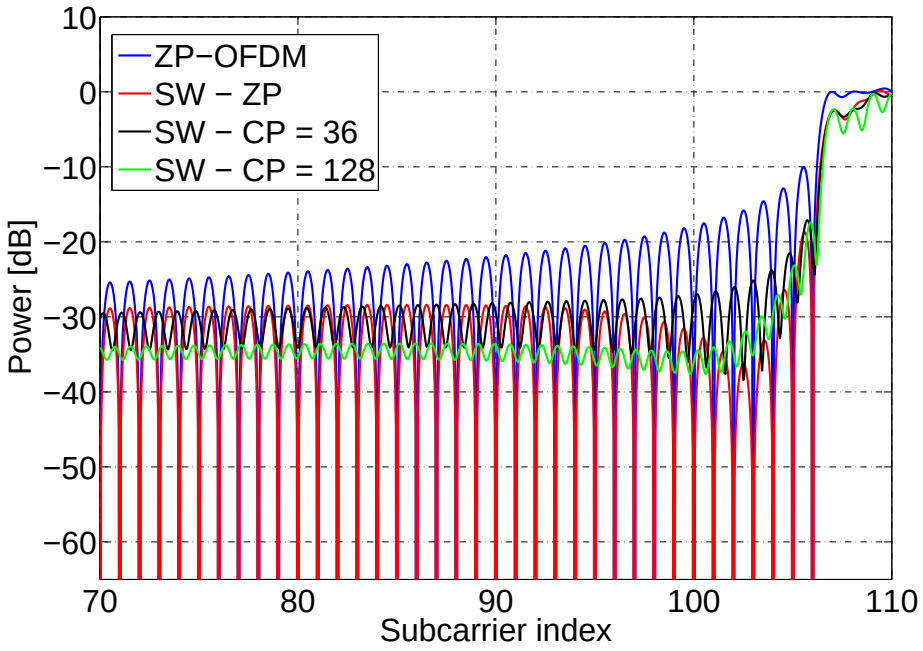

Figure 4.19: Zoomed PSD on the guard band for SW in the contiguous scenario with different CP modes.

optimization range covers all the sidelobes in the gaps. The amplitude limitation of the used nonlinear optimizer is between 0.75 and 1.25 of the original data symbol.

In Figure 4.19, the effect of CP on SW technique is investigated in the contiguous case. The performance in the ZP mode is the best and the suppression reaches -36 dB at the third sidelobe. Also with this method, the normal CP mode reduces the performance of SW compared to the ZP mode. On other hand, the extended CP mode shows better suppression performance that the normal CP mode.

Figure 4.20 shows the suppression performance of SW in the non-contiguous scenario. The performance is similar in all CP modes with slight differences. In the ZP mode, the suppression performance is -36 dB and -37 dB in 1RB and 2RB gaps, respectively. In the normal CP mode, the suppression performance is -28 dB and -40 dB in 1RB and 2RB gaps, respectively. In the extended CP mode, the suppression is -36 dB and -40 dB, correspondingly. Hence, the effect of CP is negligible in this case.

In conclusion, the CP has a destructive effect on SW in way similar to CC technique in the contiguous scenario. In the non-contiguous scenario, the suppression performance of SW in different CP modes is similar because the optimization range is extended to cover all the sidelobes in the gaps. In the normal CP mode, a clear performance reduction can be seen especially in the 1 RB gap.

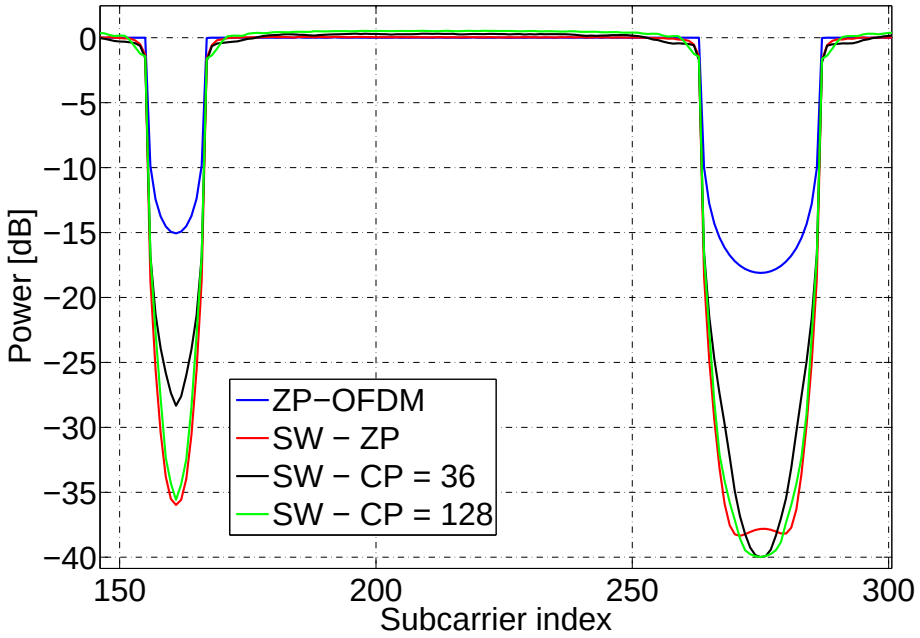

Figure 4.20: Zoomed peaks envelope of PSD on the gaps for SW in the non-contiguous scenario with different CP modes.

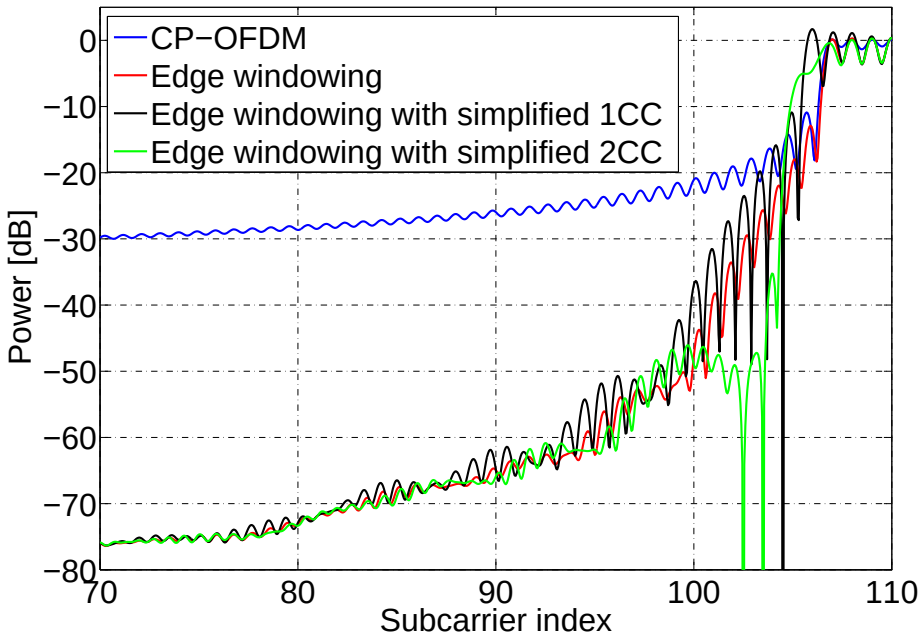

Figure 4.21: Zoomed PSD on the guard band for the combination in the contiguous scenario.

4.6 Combination of edge windowing and simplified CC

The target of the combination is to achieve better suppression while reducing the side effects. Time domain windowing techniques and PCC technique show a strong

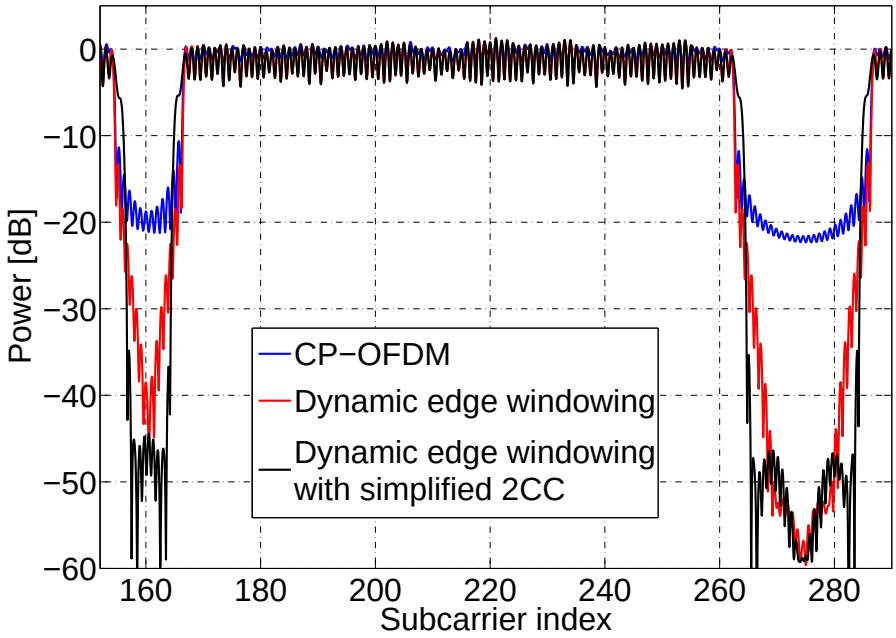

Figure 4.22: Zoomed PSD on the gaps for the combination in the non-contiguous scenario.

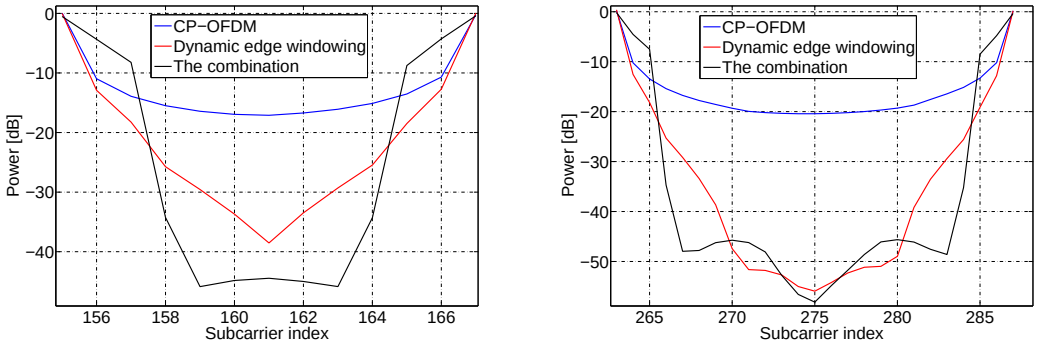

(a) 1RB gap. (b) 2RB gap.

Figure 4.23: Zoomed PSD peak envelope of the gaps for the combination using the extended CP mode.

suppression at sidelobes far from the active subcarriers. However, the suppression of CC and SW techniques is strong on the optimization range which is usually close to the active subcarriers. Therefore, the goal of the combination is to provide strong suppression all over the spectrum. As a result, the feasible combinations are time domain windowing with CC, time domain windowing with SW, time windowing with PCC, PCC with CC and PCC with SW. However, the computational complexity of SW technique is high; therefore, the combinations of SW are skipped. Regarding, PCC technique the spectral efficiency is reduced into half; therefore, it is skipped. A combination of CC and time domain windowing performance is more feasible.

The presented combinations is edge windowing with the simplified form of CC.

This combination gains the advantages of edge windowing that provides a strong suppression performance while keeping some time domain recourse to be used for mitigating channel delay spread. Moreover, simplified CC scheme has a strong suppression performance at optimization range as well as conventional CC scheme. Then, simplified CC technique helps to alleviate the required computational complexity.

The simulated performance of the combination is shown in Figure 4.21. Here the CC part of the configuration is simplified 1CC or simplified 2CC. The combination with 1CC provides a deep notch at the optimization point, but its overall performance is clearly worse than that of the edge windowing. Therefore, this combination will not be considered anymore. On the other hand, the combination with simplified 2CC suppresses effectively the PSD of all the sidelobes. The resulting level of the first sidelobe is below -35 dB.

Consequently, the combination is applied on the non-contiguous scenario where dynamic edge windowing and 2CC techniques are used together. In Figure 4.22, the resulting suppression of the combination shows clearly improved performance close to the gaps edges compared to dynamic edge windowing. Moreover, the zoomed PSD's of the gaps are depicted in Figure 4.23. The combination enhances the performance compared to dynamic edge windowing. The resulting PSD is well below -40 dB in relatively large bands around the centers of both gaps.

In conclusion, the combination of simplified 2CC with dynamic edge windowing provides an enhanced spectrum for all sidelobes, while the combination with 1CC doesn't improve the performance over dynamic edge windowing. One important notification, Equations 3.9 and 3.10 cannot be used to evaluate the matrices $\mathbf{P}$ and $\mathbf{C}$, respectively, because of windowing. Otherwise, the suppression performance of CC will be insignificant. Therefore, Equations 3.9 and 3.10 have to be updated to:

$$P_s = \sum_{k \in A} \frac{x_k (-1)^{k-k_s+1} h_k h_k^w}{\pi(1+q)(k-k_s-\frac{1}{2})[1-\pi^2\alpha^2(1+q^w)^2(k-k_s-\frac{1}{2})^2]} \tag{4.1}$$

$$C_{s,m} = \frac{(-1)^{k_m-k_s+1} h_{s,m} h_{s,m}^w}{\pi(1+q)(k_m-k_s-\frac{1}{2})[1-\pi^2\alpha^2(1+q^w)^2(k_m-k_s-\frac{1}{2})^2]}, \tag{4.2}$$

where $q^w = \frac{T_{CP}+T_w}{T_u}$ and $h_k^w = \sin(q\alpha\pi(k-k_s-0.5))$ is a periodic function changing according to active subcarrier index and the index of the optimization point.

5. PERFORMANCE EVALUATION OF THE PROPOSED SIDELOBE SUPPRESSION TECHNIQUES

The four presented techniques with their variations methods contain several compromises that limit their usage. Therefore, the performance of each technique is investigated in terms of out of band radiation, PAPR, BER, power consumption, computational complexity and throughput. The performance investigations cover the contiguous and non-contiguous scenarios with different configurations of the algorithms. Some pre-selection of the configurations was made based on the results of Chapter 4. Accordingly, the investigated configurations in the contiguous scenario are:

- Time domain windowing.
- Edge windowing.
- CC in the ZP mode: simplified 1CC, simplified 2CC, and conventional 2CC.
- CC in the extended CP mode: simplified 2CC, and conventional 2CC.
- PCC: the ZP, normal CP and extended CP modes.
- SW: the ZP, normal CP and extended CP modes.
- Edge windowing and simplified CC combination: 2CC configuration.

Similarly, the investigated configuration in the non-contiguous scenario are:

- Time domain windowing.
- Dynamic edge windowing.
- CC in the ZP mode: simplified 1CC, simplified 2CC, and conventional 2CC.
- CC in the extended CP mode: simplified 2CC, and conventional 2CC.
- Limited CC in the ZP mode: simplified 2CC, and conventional 2CC.
- PCC: the ZP, normal CP and extended CP modes.

- SW: the ZP, normal CP and extended modes.
- Edge windowing and simplified CC combination: 2CC configuration.

5.1 Out of band radiation

Out of band (OOB) radiation indicates the total power leaking outside the active subcarrier range. This indicator shows the overall performance of the technique compared to the basic OFDM scheme in the targeted suppression range illustrated in Figure 4.1. Therefore, OOB radiation values are normalized to the basic OFDM in similar mode, e.g., CC in the extended CP mode is normalized to the basic CP-OFDM in the extended CP mode. Consequently, the OOB radiation is calculated as follows:

$$P_{OOB} = \frac{\int_{f_1}^{f_2} Y(f)^2 \, df}{P_{OFDM}}, \tag{5.1}$$

where f_1 and f_2 are the frequency borders of the suppression target, $Y(f)$ is a frequency representation of the signal and P_{OFDM} is the basic OFDM power on the same interval $[f_1, f_2]$. Additionally, the power levels at specific frequency points are presented to demonstrate the strength of each suppression technique.

In the OOB calculations of the CC method, the frequency interval $[f_1, f_2]$ excludes the CC's from OOB calculation starting form the next sidelobe. The exclusion is necessary to reveal the performance of the CC method since the inserted CC power dominates the value of OOB, e.g., normalized OOB of simplified 2CC method in the contiguous scenario is 16.23 dB.

Firstly, the OOB radiation is shown in Table 5.1 for the ZP mode in the contiguous scenario. The resulting OOB radiation in the guard band is about -10 dB in all schemes except -5 dB in simplified 1CC. Moreover, the suppression of CC schemes is strong at the first sidelobe with the PSD at -41.85 dB level in the 2CC methods. PCC has strong suppression in the last sidelobe of the guard band compared to other techniques.

Secondly, Table 5.2 shows that OOB radiation of PCC and SW in the normal CP mode of the contiguous scenario. PCC technique has lower OOB compared to the ZP mode. Besides, there is a slight OOB reduction in SW compared to the ZP mode. Mainly, PCC provides better sidelobe suppression than SW.

Thirdly, the OOB radiation in the extended CP mode is shown in Table 5.3. Time domain windowing shows similar performance to edge windowing. However, there is slight reduction in suppression of edge windowing. On other hand, CC methods have similar performance with the OOB at -6.2 dB level. Generally, the PCC shows the lowest OOB radiation. The SW performance in the extended CP mode is lower than in the ZP mode. The combination shows a strong suppression

Table 5.1: Normalized OOB radiation in the contiguous scenario of the ZP mode.

Suppression Technique	OOB [dB]	1st sidelobe power [dB]	16th sidelobe power [dB]
OFDM	0	-10.26	-22.22
Simplified 1CC	-5.79	-32.77	-24.22
Simplified 2CC	-11.82	-41.85	-28.34
Conventional 2CC	-11.77	-41.85	-28.34
PCC	-9.48	-21.11	-53.88
SW	-10.78	-19.99	-28.55

Table 5.2: Normalized OOB radiation in the contiguous scenario of the normal CP mode.

Suppression Technique	OOB [dB]	1st sidelobe power [dB]	16th sidelobe power [dB]
OFDM	0	-10.79	-25.43
PCC	-7.75	-20.27	-42.68
SW	-7.29	-17.06	-28.22

Table 5.3: Normalized OOB radiation in the contiguous scenario of the extended CP mode.

Suppression Technique	OOB [dB]	1st sidelobe power [dB]	16th sidelobe power [dB]
OFDM	0	-11.69	-27.11
Time domain windowing	-5.56	-12.74	-66.41
Edge windowing	-5.55	-12.74	-66.41
Simplified 2CC	-6.19	-31.48	-29.08
Conventional 2CC	-6.18	-31.48	-29.08
PCC	-1.55	-16.58	-32.26
SW	-8.90	-17.44	-33.65
The combination	-27.43	-34.9	-63.27

in the first and in the 16th sidelobes and in the overall OOB radiation which is the highest compared to other techniques.

Fourthly, the non-contiguous scenario for the ZP mode is investigated in Table

Table 5.4: Normalized OOB radiation in the non-contiguous scenario of the ZP mode.

Suppression Technique	OOB at 1RB [dB]	OOB at 2RB [dB]	1st sidelobe power at 1RB gap [dB]	1st sidelobe power at 2RB gap [dB]	Middle sidelobe power at 1RB gap [dB]	Middle sidelobe power at 2RB gap [dB]
OFDM	0	0	-9.93	-15.02	-15.02	-18.12
Simplified 1CC	-11.89	-6.93	-25.96	-30.09	-24.11	-22.16
Simplified 2CC	-5.57	-15.80	-20.21	-28.26	20.28	-35.95
Conventional 2CC	-32.38	-15.95	-44.85	-42.21	-42.11	-29.72
Limited simplified 2CC	-9.41	-12.78	-21.31	-28.34	-27.16	-28.24
Limited conventional 2CC	-24.28	-13.15	-42.45	-41.11	-35.39	-27.53
PCC	-14.08	-15.00	-20.62	-20.62	-38.26	-47.14
SW	-12.07	-12.48	-19.09	-18.74	-35.98	-37.82

Table 5.5: Normalized OOB radiation in the non-contiguous scenario of the normal CP mode.

Suppression Technique	OOB at 1RB [dB]	OOB at 2RB [dB]	1st sidelobe power in both gaps [dB]	Middle sidelobe power at 1RB gap [dB]	Middle sidelobe power at 2RB gap [dB]
OFDM	0	0	-10.62	-17.6	-21.04
PCC	-12.12	-12.70	-20.3	-34.01	-37.1
SW	-8.42	-9.49	-16.78	-28.36	-40.44

5.4. The results show that the conventional 2CC leaks the lowest OOB, where the performance is focused at the 1st sidelobes. On other hand, there are reduction on the suppression performance of limited conventional 2CC that is resulted from power limitation on the CC's. PCC shows strong suppression in both gaps resulting in the strongest suppression at the middle sidelobes. On other hand, SW achieves

Table 5.6: Normalized OOB radiation in the non-contiguous scenario of the extended CP mode.

Suppression Technique	OOB at 1RB [dB]	OOB at 2RB [dB]	1st sidelobe power at 1RB gap [dB]	1st sidelobe power at 2RB gap [dB]	Middle sidelobe power at 1RB gap [dB]	Middle sidelobe power at 2RB gap [dB]
OFDM	0	0	-11.57	-11.57	-20.08	-23.05
Time domain windowing	-4.85	-5.74	-12.74	-12.74	-37.81	-57.39
Dynamic edge windowing	-4.85	-5.74	-12.74	-12.74	-39.81	-56.66
Simplified 2CC	-6.84	-7.81	-18.05	-21.59	-28.77	-26.94
Conventional 2CC	-11.93	-7.51	-24.87	-23.88	-27.88	-26.5
PCC	-4.97	-5.03	-16.45	-16.45	-24.99	-28
SW	-8.46	-9.16	-16.78	-16.78	-35.64	-40.01
The combination	-24.73	-26.17	-34.7	-34.92	-58.67	-44.3

strong suppression specially at the middle of the gap. Simplified 1CC yields sufficient suppression with PSD at -25.96 dB and -30.09 dB in the first sidelobe of 1RB and 2RB gaps, respectively.

Fifthly, OOB radiation is investigated in Table 5.5 for the non-contiguous scenario of the normal CP mode. The resulting suppression of PCC and SW is less than the resulting suppression in the ZP mode. Basically, PCC has better suppression than SW.

Sixthly, Table 5.6 shows the OOB radiation for different techniques in the non-contiguous scenario of the extended CP mode. The results of time domain windowing are similar. The OOB radiation in 1RB gap is -6.8 dB and -11.9 dB for simplified and conventional 2CC scheme, respectively. The OOB radiation of 2RB gap is -7.8 dB and -7.5 dB for simplified and conventional schemes, respectively. However, suppression performance is stronger at the first lobe in conventional than simplified. But simplified 2CC scheme has better suppression in the middle sidelobe of the gap. On other hand, PCC has the worse performance in the non-contiguous scenario compared to the ZP mode because of CP impact. Mainly, the combination performs the best compared to other techniques.

The OOB radiation shows the general performance of different techniques. Therefore, the power of 1st sidelobe peaks and middle sidelobes peak are important to understand the sidelobes pattern after using this indicator. The OOB radiation of time domain windowing methods is small compared to other techniques because of the weak suppression of time domain windowing techniques in sidelobes close to active subcarriers. Consequently, the close sidelobes contains a high power levels that increases the value of OOB indicator. Hence, OOB indicator shows the suppression differences between different configurations of the same technique. Mainly, the combination method shows the strongest performance on all sidelobes in the spectrum, either in the guard bands or in the gaps.

5.2 PAPR impact

The used techniques modify the signal in time domain in such a way that they reshape the OFDM symbol, insert weighted carriers, or re-weight the subcarriers. Therefore, there is a possibility to increase the PAPR of the OFDM system. As a result, the PAPR has to be investigated for each used suppression technique.

The PAPR of the OFDM signal is calculated as follows:

$$PAPR = \frac{\max|y_k|^2}{\frac{1}{N}\sum_{k=1}^{N}|y_k|^2}. \tag{5.2}$$

Accordingly, the PAPR of basic OFDM the CP normal mode and CP extended mode are expected to be the same as CP's are just copied samples. Hence neither the average nor the peak power change. Nevertheless, the ZP mode has a zero guard interval, which reduces the average power of the signal. Hence, the resulting PAPR in the ZP mode is expected to increase, while the peak power remains the same. Generally, the effects of each sidelobe control method on the PAPR are similar in the contiguous and non-contiguous scenarios. Therefore, the PAPR presented for each technique shows the PAPR effect in both, contiguous and non-contiguous scenarios.

Figure 5.1 shows the PAPR of the different suppression techniques in different CP modes and configurations. As expected, the PAPR of ZP-OFDM is higher than CP-OFDM in the normal and extended CP modes. Therefore, PAPR is expected to increase for techniques applied on ZP-mode. In time domain windowing techniques, the resulting PAPR has a slight increment compared to basic OFDM in extended mode. In CC techniques, the used CC schemes including simplified 1CC, simplified 2CC, conventional 2CC, limited simplified 2CC and limited conventional 2CC behave similar to PAPR of basic OFDM Due to the small number of used CC's compared to number of active subcarriers. Similarly, PAPR of SW technique in the

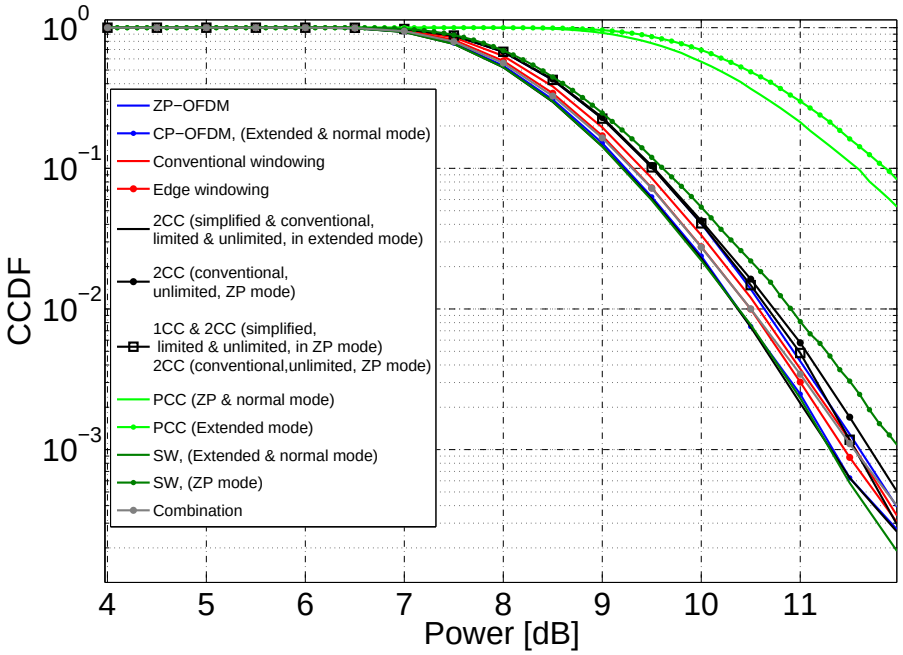

Figure 5.1: PAPR of time windowing techniques, CC, PCC, SW in different schemes and CP modes.

normal and extended CP modes follows the performance of the basic OFDM in the normal and extended CP modes, respectively. The combination technique has an corresponding impact as edge windowing since it is a combination of edge windowing and simplified 2CC. Nevertheless, PCC technique results in high increment in PAPR because of windowing impact of PCC in time domain.

5.3 CC power levels

The represented techniques don't change the power consumption of the OFDM signal except CC technique that requires extra power for the weight vector $\mathbf{g}$ in Problem (3.11). Therefore in the simulations of CC method, the OFDM symbol is normalized in the following way:

$$A = \frac{||\mathbf{x}||^2}{||\mathbf{x}||^2 + ||\mathbf{g}||^2}, \tag{5.3}$$

where $\mathbf{x} = [x_0, x_1, ..., x_{N-1}]$ is the parallel data samples of the OFDM symbols and the normalization factor A belongs to $(0, 1)$. As a result, Equation (2.2) is rewritten in the following way:

$$y_{norm}(t) = \sqrt{A}\left[\sum_{k=0}^{N-1} x_k \exp[j2\pi f_k t] + \sum_{m \in Z} g_m \exp[j2\pi f_m t]\right], \tag{5.4}$$

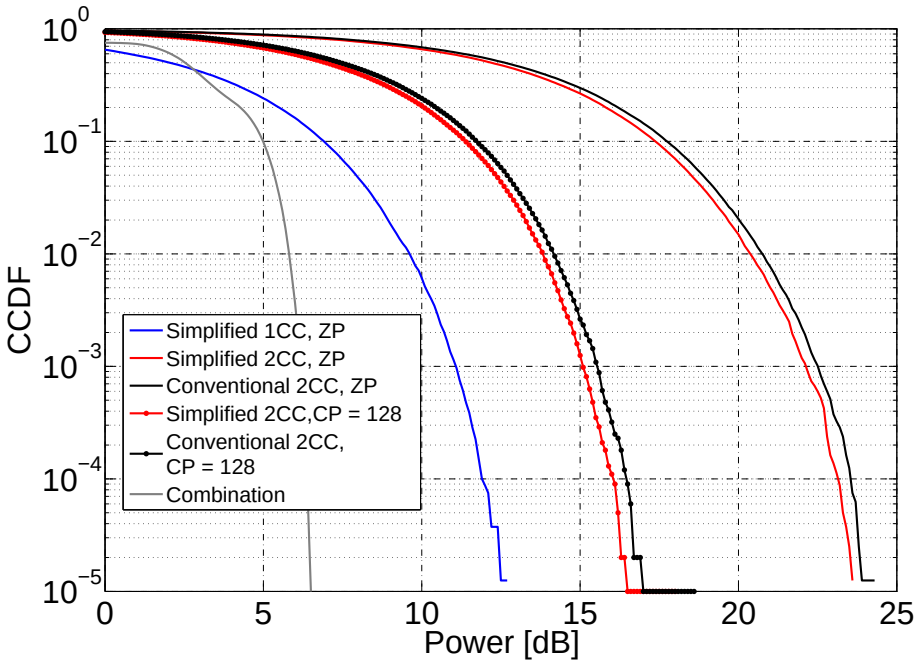

Figure 5.2: A 2CC scheme with CC power levels equal to the active subcarriers correspond to the 6 dB point on the power axis.

where Z is the indexes set of the IFFT input for CC's and $[f_1, f_2, ..., f_M]$ are the center frequencies of the CC's. Hence, samples power in the vector $\mathbf{x}$ is reduced resulting in degradation in BER performance.

Figure 5.2 and Figure 5.3 show the CCDF of the power consumption over weight vector $\mathbf{g}$ for different CC schemes in the ZP and CP modes of the contiguous and non-contiguous scenarios, respectively. The power consumption is the lowest in the combination compared to other CC schemes. The simulations explains the need for power limitation in 2CC schemes. The limitation of the signal prohibits the signal from exceeding the power in the simplified and conventional schemes.

5.4 BER reduction

Some of the used techniques require increased transmission power in order to suppress the sidelobes. As a result, the BER is expected to increase reducing the efficiency of the system. Figure 5.4 illustrates the BER of the represented techniques in different CP modes for the contiguous scenario. The resulting BER of time domain windowing, edge windowing and PCC in all of the CP modes is not affected. Nevertheless, CC schemes increase the BER of the system depending on the power consumption over the CC's. Simplified 1CC has corresponding BER to OFDM because of the small power consumption. There is a small increment in BER of simplified 2CC and conventional 2CC compared to OFDM in the ZP mode. Besides the BER of simplified 2CC and conventional 2CC is close to BER of OFDM

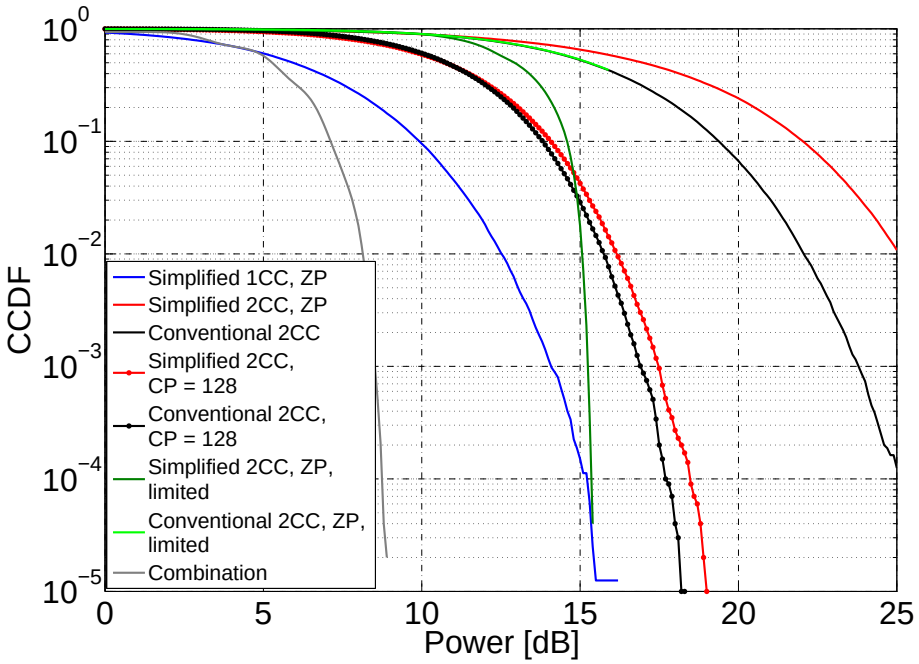

Figure 5.3: A 2CC scheme with CC power levels equal to the active subcarriers correspond to the 9 dB point on the power axis.

in the extended CP mode. Moreover, the combination results in matching BER to OFDM BER. Regarding SW, there there is a clear degradation in the BER performance. Though the power of SW equals the power of OFDM, the SW modifies the subcarriers amplitudes causing errors in the detection. Therefore, reducing the constraint range of the subcarriers amplitudes degrades the BER. But, the suppression performance will degrade as well.

In the non-contiguous scenario, the edge windowing, time domain windowing and PCC have identical BER to basic OFDM in all CP modes as shown in Figure 5.5. Moreover, the performance of simplified 1CC and the combination is similar to the BER of the basic OFDM. Simplified 2CC and conventional 2CC methods have a slight increase in BER in the extended CP mode. Furthermore, the limited CC schemes have a small BER increment because of the power limitation added to the optimization. However, there are notable increment in BER in simplified and conventional 2CC in the ZP mode. Similarly, the BER of SW has high BER compared to OFDM due to weights added to the subcarriers.

In the simulations, the BER is evaluated versus the SNR. As a result, the BER results don't change as the CP mode changes. In fact, for constant SNR value, the energy per transmitted bit increases with increasing CP length. In other words, for constant E_b/N_o ratio, the BER performance is reduced with increased CP length. The difference in energy per transmitted bit between the normal and extended CP modes is about 0.67 dB.

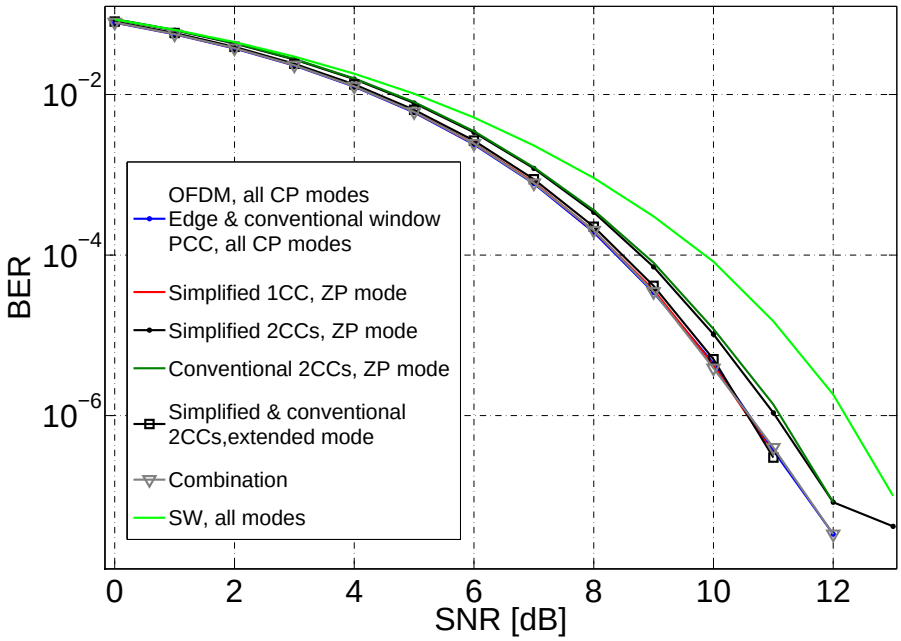

Figure 5.4: BER vs. SNR of time windowing techniques, CC, PCC, SW in different CP modes and configurations in the contiguous scenario.

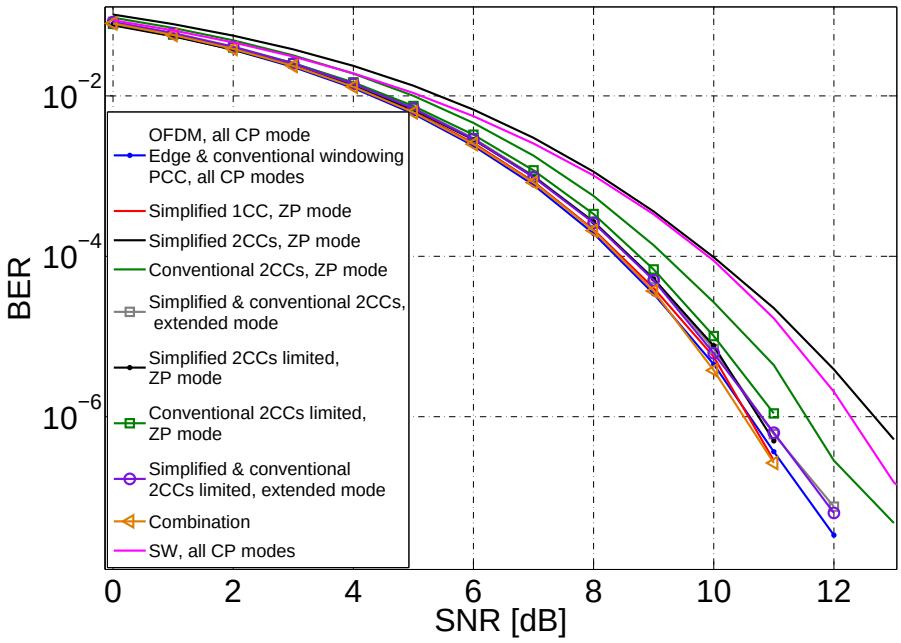

Figure 5.5: BER vs. SNR of time windowing techniques, CC, PCC, SW in different CP modes and configurations in the non-contiguous scenario.

5.5 Added computational complexity

The number of operations required for the suppression technique may have a significant impact on the overall complexity of an OFDM transmitter. The computational

complexity of each technique is investigated numerically based on the equations given in Chapter 2 and Appendix A. The computational complexities of time windowing techniques and PCC techniques are the same for the contiguous and non-contiguous scenarios. But CC and SW techniques have different computational complexity in different scenarios because of the variations in the number of CC's and/or optimization points, as discussed in Chapter 4. The computational complexity of SW is not calculated because of the intensive complexity required to solve for the weights due to the high number of iterations required.

Table 5.7 summarizes the required computational complexity for all the techniques in different configurations. The complexity is expressed as the number of additional real arithmetic operations (multiplications, additions, divisions, square roots) per transmitted OFDM symbol due to each sidelobe suppression method. The PCC technique shows the lowest computational complexity, 150 multiplications only. Time domain windowing requires a small number of computations, 184 multiplications and 96 additions per OFDM symbol. Nevertheless, edge windowing shows a clear increase in the computational complexity. In fact, the increment in the edge windowing results mostly from the use of extra IFFT block as discussed in Section 3.1. The computational complexity of the extra IFFT is 3076 multiplications and 12292 additions. The additional complexity due to windowing operation is 248 multiplications and 125 additions, in case of the edge windowing method. Similarly, the combination of dynamic edge windowing and CC needs an extra IFFT in addition to the operations needed for the simplified 2CC method. Hence, the additional computational complexity of the combination, without considering the IFFT block, is 6008 multiplications and 4808 additions in the contiguous scenario and 12168 multiplications and 9752 additions in the non-contiguous scenario. Regarding the CC schemes, the calculated computational complexity of the simplified schemes are less than the conventional schemes.

In Table 5.8, the required computational complexity in the different CC schemes is investigated. The resulting computational complexity of simplified scheme is multiplied by two and four in the contiguous scenario and non-contiguous scenarios, respectively. The reason of the multiplication that the simplified methods breaks the optimization problem into smaller problems. The simplified scheme doesn't show reduction in the computations of matrix $\mathbf{P}$ because of the linear relation between the required computations and the number of optimization points. Similarly, the computational complexity of matrix $\mathbf{C}$ is linear with the number of the CC's and optimization range. Hence, the conventional and simplified 2CC schemes have similar computational complexity of the matrices $\mathbf{C}$ and $\mathbf{P}$. However, the difference appears in weight evaluation process and pseudo inverse calculation, especially when the size of $\mathbf{C}$ and $\mathbf{P}$ increases. Moreover, the reduction caused by simplified

Table 5.7: Additional computational complexity due to the considered sidelobe control methods.

Suppression technique	No. multipliers	No. adders	No. divisions	No. square roots
Time domain windowing	184	96	0	0
Dynamic or normal edge windowing	3324	12417	0	0
Simplified 1CC contiguous	1200	1800	602	0
Simplified 1CC non-contiguous	2408	3612	1204	0
Simplified 2CC contiguous	2408	3608	1200	0
Simplified 2CC non-contiguous	4920	7336	2432	0
Conventional 2CC contiguous	2416	3616	1200	0
Conventional 2CC non-contiguous	6072	8536	2528	0
Limited simplified 2CC non-contiguous	5644	8028	2516	32
Limited conventional 2CC non-contiguous	28510	31148	2633	44
PCC	150	0	0	0
The combination, contiguous	9332	17225	1204	0
The combination, non-contiguous	15492	22169	16320	0

methods is stronger when power limitation is considered in SVD calculation that there is more than 20000 multiplications are reduced.

Regarding the complexity of SW, the technique requires an intensive number of computations in order to solve for subcarriers weights, as 1000 iterations are used to evaluate the subcarriers weights. A clear example of the required computational complexity is that the creation of the matrix $\mathbf{S}$ in the optimization Problem (3.15) requires 15840 multiplications, 23760 additions and 7920 divisions.

Table 5.8: Detailed computational complexity of different CC configurations.

Scheme	Configuration	Operation	**P** evaluation	**C** evaluation	Weights optimization	Pseudo inverse or SVD of **C**
Simplified	1CC contiguous	$\mathcal{C}$	1200	0	0	0
		$\mathcal{A}$	1800	0	0	0
		$\mathcal{D}$	600	0	2	0
	1CC non-contiguous	$\mathcal{C}$	2400	8	0	0
		$\mathcal{A}$	3600	12	0	0
		$\mathcal{D}$	1200	4	4	0
	2CC contiguous	$\mathcal{C}$	2400	0	8	0
		$\mathcal{A}$	3600	0	8	0
		$\mathcal{D}$	1200	0	0	0
	2CC non-contiguous	$\mathcal{C}$	4800	32	16	72
		$\mathcal{A}$	7200	48	16	72
		$\mathcal{D}$	2400	16	0	16
	Limited 2CC non-contiguous	$\mathcal{C}$	4800	32	168	644
		$\mathcal{A}$	7200	48	160	620
		$\mathcal{D}$	2400	16	56	44
		$\mathcal{S}$	0	0	0	32
Conventional	2CC contiguous	$\mathcal{C}$	2400	0	16	0
		$\mathcal{A}$	3600	0	16	0
		$\mathcal{D}$	1200	0	0	0
	2CC non-contiguous	$\mathcal{C}$	4800	192	64	1080
		$\mathcal{A}$	7200	128	64	1080
		$\mathcal{D}$	2400	64	0	64
	Limited 2CC non-contiguous	$\mathcal{C}$	4800	192	252	23330
		$\mathcal{A}$	7200	128	190	23566
		$\mathcal{D}$	2400	64	50	119
		$\mathcal{S}$	0	0	0	44

5.6 Spectral efficiency

The presented techniques consume time and/or frequency resources, which reduces the total throughput and spectral efficiency of the system. Basically, the different CP modes use different time resources in CP. The normal CP and the ZP modes use 6.6% for guard interval, while the extended CP mode uses 20% of time resource. In other words, the ZP and normal CP modes can support 13.4% higher data rate than the extended CP mode. These results are applicable on all presented techniques on different CP modes.

The CC technique exploits an empty frequency space in order to achieve the suppression. This reduces the total throughput of the system. However in the represented CC schemes, the number of employed subcarriers is small compared to the number of active subcarriers. Therefore, the reduction in throughput is negligible. SW doesn't require any additional time or frequency resources. On other hand, the PCC technique depends on duplicating the data symbols. As a result, the spectral efficiency is reduced to the half.

6. CONCLUSION

The simulations results in Chapter 4 represent the suppression performance of each technique in the contiguous and non-contiguous scenarios of 5 MHz 3GPP LTE. Then, the limitations of each technique are illustrated in Chapter 5. The main objective of the thesis is achieved by using the combination of dynamic edge windowing and simplified 2CC techniques. The simulations show that lower than -45 dB power level is achieved in both the guard bands and gaps using the combination. Furthermore, the PAPR or BER are not affected.

Generally, the CP has a minor impact on the OFDM spectrum. However, the techniques, which depend on sidelobe prediction, are affected by the length of CP. Basically, CC and SW techniques suppress the unwanted sidelobes by the sidelobes of the weighted subcarriers. As a result, the modification in the ratio of the CP length to the useful symbol length shifts the peaks of sidelobes so that it degrades the suppression performance of CC and SW, especially the normal CP mode. The suppression performance of the CC and SW in the extended CP mode is improved compared to the normal CP mode. On other hand, conventional time domain windowing and edge windowing are not affected negatively by the CP length since they require further extension in time domain.

Concerning the limitations of the represented techniques, the chosen configurations cause a slight increase in PAPR and slightly reduced BER performance compared to the basic CP-OFDM. However, the PCC method results in a significant increase in the PAPR. Regarding the computational complexity, CC and SW techniques require larger number of computations compared to time domain windowing and PCC techniques since they depend on solving minimization problems. Therefore, the simplified CC method is proposed, showing an efficient reduction in the computational complexity especially in the power limited schemes of CC.

The time windowing technique has the potential of being combined with other techniques since time windowing has low computational complexity. On other hand, CC technique uses LLS optimization method requiring large number of computational complexity especially when the limitation applied. Hence, improved methods for solving the optimization problem are required to reduce the computational complexity.

BIBLIOGRAPHY

[1] M. Shafi, A. Hashimoto, M. Umehira, S. Ogose, and T. Murase, "Wireless communications in the twenty-first century: a perspective," *Proceedings of the IEEE*, vol. 85, no. 10, pp. 1622–1638, 1997.

[2] H. Mahmoud, T. Yucek, and H. Arslan, "OFDM for cognitive radio: merits and challenges," *Wireless Communications, IEEE*, vol. 16, no. 2, pp. 6–15, 2009.

[3] K. Balachandran, K. Budka, T. Chu, T. Doumi, and J. Kang, "Mobile responder communication networks for public safety," *Communications Magazine, IEEE*, vol. 44, no. 1, pp. 56–64, 2006.

[4] M. Faulkner, "The effect of filtering on the performance of OFDM systems," *Vehicular Technology, IEEE Transactions on*, vol. 49, no. 5, pp. 1877–1884, 2000.

[5] T. Weiss, J. Hillenbrand, A. Krohn, and F. Jondral, "Mutual interference in OFDM-based spectrum pooling systems," in *Proc. IEEE Vehicular Technology Conference (VTC 2004-Spring)*, May 2004, pp. 1873–1877.

[6] A. Sahin and H. Arslan, "Edge Windowing for OFDM Based Systems," *Communications Letters, IEEE*, vol. 15, no. 11, pp. 1208–1211, 2011.

[7] S. Brandes, I. Cosovic, and M. Schnell, "Sidelobe suppression in OFDM systems by insertion of cancellation carriers," in *Proc. IEEE Vehicular Technology Conference (VTC-2005-Fall)*, Sep. 2005, pp. 152–156.

[8] I. Cosovic, S. Brandes, and M. Schnell, "Subcarrier weighting: a method for sidelobe suppression in ofdm systems," *Communications Letters, IEEE*, vol. 10, no. 6, pp. 444–446, 2006.

[9] K. Panta and J. Armstrong, "Spectral analysis of OFDM signals and its improvement by polynomial cancellation coding," *Consumer Electronics, IEEE Transactions on*, vol. 49, no. 4, pp. 939–943, 2003.

[10] H. Mahmoud and H. Arslan, "Sidelobe suppression in OFDM-based spectrum sharing systems using adaptive symbol transition," *Communications Letters, IEEE*, vol. 12, no. 2, pp. 133–135, 2008.

[11] I. Cosovic and T. Mazzoni, "Sidelobe Suppression in OFDM Spectrum Sharing Systems Via Additive Signal Method," in *Proc. IEEE Vehicular Technology Conference (VTC2007-Spring)*, April 2007, pp. 2692–2696.

[12] S. Pagadarai, R. Rajbanshi, A. M. Wyglinski, and G. Minden, "Sidelobe Suppression for OFDM-Based Cognitive Radios Using Constellation Expansion," in *Proc. IEEE Wireless Communications and Networking Conference (WCNC 2008)*, April 2008, pp. 888–893.

[13] W. Zou and Y. Wu, "COFDM: an overview," *Broadcasting, IEEE Transactions on*, vol. 41, no. 1, pp. 1–8, 1995.

[14] M. Pun, M. Morelli, and C. Kuo, *Multi-Carrier Techniques For Broadband Wireless Communications: A Signal Processing Perspectives.* Imperial College Press, 2007.

[15] Y. Shmaliy, *Continuous-Time Signals.* Springer, 2006.

[16] J. A. C. Bingham, "Multicarrier modulation for data transmission: an idea whose time has come," *Communications Magazine, IEEE*, vol. 28, no. 5, pp. 5–14, 1990.

[17] S. Mitra, *Digital Signal Processing: A Computer-based Approach.* McGraw-Hill, 2010.

[18] P. Diaconis, "Average running time of the fast fourier transform," *Journal of Algorithms*, vol. 1, no. 2, pp. 187 – 208, 1980.

[19] M. Ivrlac and J. Nossek, "Influence of a Cyclic Prefix on the Spectral Power Density of Cyclo-Stationary Random Sequences," in *Multi-Carrier Spread Spectrum 2007.* Springer, 2007, vol. 1, pp. 37–46.

[20] S. H. Han and J. H. Lee, "An overview of peak-to-average power ratio reduction techniques for multicarrier transmission," *Wireless Communications, IEEE*, vol. 12, no. 2, pp. 56–65, 2005.

[21] J. Proakis, *Communication systems engineering.* Prentice Hall PTR, 2002.

[22] P. Stoica and R. Moses, *Spectral analysis of signals.* Pearson Prentice Hall, 2005.

[23] P. D. Welch, "The use of fast Fourier transform for the estimation of power spectra: A method based on time averaging over short, modified periodograms," *Audio and Electroacoustics, IEEE Transactions on*, vol. 15, no. 2, pp. 70–73, 1967.

[24] M. S. Bartlett, "Smoothing Periodograms from Time-Series with Continuous Spectra," *Nature (London)*, vol. 161, no. 4096, pp. 686–687, 1967.

[25] T. van Waterschoot, V. Le Nir, J. Duplicy, and M. Moonen, "Analytical Expressions for the Power Spectral Density of CP-OFDM and ZP-OFDM Signals," *Signal Processing Letters, IEEE*, vol. 17, no. 4, pp. 371–374, 2010.

[26] A. Loulou and M. Renfors, "Effective Schemes for OFDM Sidelobe Control in Fragmented Spectrum Use," in *Proc. IEEE Personal, Indoor and Mobile Radio Communications (PIMRC'13)*, Sep. 2013, pp. 471–475.

[27] A. Sahin and H. Arslan, "The Impact of Scheduling on Edge Windowing," in *Proc. Global Telecommunications Conference (GLOBECOM 2011)*, Dec. 2011, pp. 1–5.

[28] R. Airoldi, F. Garzia, and J. Nurmi, "Efficient FFT pruning algorithm for non-contiguous OFDM systems," in *Proc. IEEE Design and Architectures for Signal and Image Processing (DASIP)*, Nov. 2011, pp. 1–6.

[29] L. Baltar, F. Schaich, M. Renfors, and J. Nossek, "Computational complexity analysis of advanced physical layers based on multicarrier modulation," in *Proc. Future Network Mobile Summit (FutureNetw)*, June 2011, pp. 1–8.

[30] A. Loulou, S. Afrasiabi Gorgani, and M. Renfors, "Enhanced OFDM Techniques for Fragmented Spectrum Use," in *Proc. Future Network and Mobile Summit (FutureNetw)*, July 2013, p. 10.

[31] W. Gander, "Least Squares with a Quadratic Constraint," *Numer. Math.*, vol. 36, pp. 291–307, 1981.

[32] M. El-Saadany, A. Shalash, and M. Abdallah, "Revisiting active cancellation carriers for shaping the spectrum of OFDM-based Cognitive Radios," in *Proc. IEEE Sarnoff Symposium (SARNOFF '09)*, April 2009, pp. 1–5.

[33] H. Mahmoud and H. Arslan, "Spectrum shaping of OFDM-based cognitive radio signals," in *Proc. IEEE Radio and Wireless Symposium (RWS 2008)*, Jan. 2008, pp. 113–116.

[34] Z. Yuan, S. Pagadarai, and A. M. Wyglinski, "Cancellation carrier technique using genetic algorithm for OFDM sidelobe suppression," in *Proc. IEEE Military Communications Conference (MILCOM 2008)*, Nov. 2008, pp. 1–5.

[35] S. Brandes, I. Cosovic, and M. Schnell, "Reduction of out-of-band radiation in OFDM systems by insertion of cancellation carriers," *Communications Letters, IEEE*, vol. 10, no. 6, pp. 420–422, 2006.

[36] J. Armstrong, P. M. Grant, and G. Povey, "Polynomial cancellation coding of OFDM to reduce intercarrier interference due to Doppler spread," in *Proc IEEE Global Telecommunications Conference (GLOBECOM 1998)*, Nov. 1998, pp. 2771–2776.

[37] R. Fletcher, *Practical methods of optimization; (2nd ed.)*. Wiley-Interscience, 1987.

A. CANCELLATION CARRIER SOLUTION AND REQUIRED COMPUTATIONAL COMPLEXITY

CC technique uses LLS equation to evaluate the required weights. Therefore, it is important to define the solution of optimization problem in Equation (3.11) for different CC schemes. Beside, the required computations for collecting the matrices are considered in this chapter in different possible situations.

A.1 Linear least squares solution and required computational complexity

LLS solution provides the minimum required input parameters to get the minimum possible output in CC technique. Alternatively, other solutions with higher complexity and more accuracy may be used likewise genetic algorithms and nonlinear optimization. But, the concerns of computational complexity in this document leads to the use of least squares solutions.

In this section, the used algorithm for solving the LLS problems are investigated showing the required arithmetics. Furthermore, a quadratic constrained is important to be considered in these problems, to keep the power used in the solution under a power limits.

A.1.1 Linear least squares solution

Consider the problem of finding vector $\mathbf{x} \in \mathbf{R}^n$, where $\mathbf{R}^n$ denotes the vector space of real n-vectors, is given in the following way:

$$\mathbf{A}\mathbf{x} = \mathbf{b}, \tag{A.1}$$

where data matrix $\mathbf{A} \in \mathbf{R}^{n \times m}$ and the observation vector $\mathbf{b} \in \mathbf{R}^m$. If $m \geq n$, then there are more equations than the unknowns and the Equation (A.1) is called overdetermined system. Usually, overdetermined systems have more than one solution, e.g., when $\mathbf{A}$ is a full rank matrix. Consequently, Equation (A.1) can be reformulated as follows:

$$\min_{\mathbf{x}} ||\mathbf{A}\mathbf{x} - \mathbf{b}||^2. \tag{A.2}$$

The method used to solve the Problem (A.2) is the normal equations method.

Mainly, the condition $\mathbf{rank}(\mathbf{A}) = n$ is required to obtain at least one solution. Consequently, the solution of $\mathbf{x}$ is represented as follows:

$$\mathbf{x} = (\mathbf{A}^T\mathbf{A})^{-1}\mathbf{A}^T\mathbf{b}. \tag{A.3}$$

The parameters in the Problem (A.1) is corresponding to the Problem (3.11). As a result, data matrix $\mathbf{A}$ is corresponding to matrix $\mathbf{C}$, observation vector $\mathbf{b}$ is corresponding to vector $-\mathbf{P}$, variable vector $\mathbf{x}$ is corresponding to vector $\mathbf{g}$, the number of unknowns n is corresponding to number of CC's M and the number of equations m is corresponding to number of optimization points S. Hence the solution to Problem (3.11) without constraints is defined as follows:

$$\mathbf{g} = (\mathbf{C}^T\mathbf{C})^{-1}\mathbf{C}^T(-\mathbf{P}), \tag{A.4}$$

where the condition $\mathbf{rank}(\mathbf{C}) = M$ is applied. The part $(\mathbf{C}^T\mathbf{C})^{-1}\mathbf{C}^T$ represents the pseudo inverse of the matrix $\mathbf{C}$. This part is constant in fixed CC scenarios. Consequently, this part is computed once, but it is computed per configuration in the dynamic scenarios of CC. The computational complexity required to compute pseudo inverse of the matrix $\mathbf{C}$ involves the computational complexity of two multiplication and one inverse of $M \times M$ matrix. Generally, multiplying the matrix $\mathbf{A}^{m\times n}$ by matrix $\mathbf{B}^{n\times o}$ requires the following number of computations:

$$\begin{aligned} \mathcal{C} &= mno \\ \mathcal{A} &= mno \end{aligned} . \tag{A.5}$$

Gauss-Jordan algorithm is used to compute the inverse of the matrix. Therefore, the required computational complexity to find the inverse of square matrix $\mathbf{A}^{n\times n}$ is:

$$\begin{aligned} \mathcal{C} &= n^2 - n \\ \mathcal{A} &= n^2 - n \\ \mathcal{D} &= n^2 \end{aligned} . \tag{A.6}$$

Then, Equations (A.5) and (A.6) are applied to find the required complexity of the pseudo inverse of the matrix $\mathbf{C}^{S\times M}$ as follows:

$$\begin{aligned} \mathcal{C} &= 2SM^2 + M^2 - M \\ \mathcal{A} &= 2SM^2 + M^2 - M \\ \mathcal{D} &= M^2 \end{aligned} , \tag{A.7}$$

where $\mathcal{D}$ is the number of divisions required. Then, the computational complexity of the whole system is calculated after multiplying vector $-\mathbf{P}$ by the pseudo inverse

of matrix $\mathbf{C}$. As a result, the computational complexity of dynamic and unlimited CC scheme is computed in the following way:

$$\begin{aligned} \mathcal{C} &= 2SM^2 + SM + M^2 - M \\ \mathcal{A} &= 2SM^2 + SM + M^2 - M \\ \mathcal{D} &= M^2 \end{aligned} . \tag{A.8}$$

Consequently, the computational complexity of fixed and unlimited CC scheme is evaluated as follows:

$$\begin{aligned} \mathcal{C} &= SM \\ \mathcal{A} &= SM \end{aligned} . \tag{A.9}$$

A.1.2 Linear least squares with quadratic constraint solution

Considering the Problem (A.2) again, it is possible that the resulting solution from Problem (A.4) without limitation has a high power value of the variable vector $\mathbf{x}$. Therefore, it is necessary for many cases to limit the power of $\mathbf{x}$ to certain level. Consequently, power constraint is added to the Problem (A.2) in the following way:

$$\min_{\mathbf{x}} ||\mathbf{Ax} - \mathbf{b}||^2 \text{ subject to } ||\mathbf{x}||^2 \leq a^2, \tag{A.10}$$

where a^2 is the power limit of variable x. Problem (A.10) is reformulated using the Lagrangian function L and Lagrangian multiplier λ as follows:

$$L(\mathbf{x}, \lambda) = ||\mathbf{Ax} - \mathbf{b}||^2 + \lambda[||\mathbf{x}||^2 - a^2]. \tag{A.11}$$

Therefore the solution is in solving for the normal equations $\frac{\partial L}{\partial \mathbf{x}} = \mathbf{0}$ and $\frac{\partial L}{\partial \lambda} = 0$. Then, the solution can be found by using the following algorithm:

$$
\begin{aligned}
&\text{Compute the SVD } \mathbf{A} = \mathbf{U}\mathbf{\Sigma}\mathbf{V}^T \\
&\mathbf{V} = [\mathbf{v}_1, ..., \mathbf{v}_n] \\
&\mathbf{b} = \mathbf{U}^T\mathbf{b} \\
&r = rank(\mathbf{A}) \\
&\text{if } \sum_{i=1}^{r} \left(\frac{b_i}{\sigma_i}\right)^2 > a^2 \\
&\qquad \text{Solve for } \lambda \text{ where, } \sum_{i=1}^{r} \left(\frac{\sigma_i b_i}{\sigma_i^2 + \lambda}\right)^2 = a^2 \ , \qquad \text{(A.12)} \\
&\qquad \mathbf{x} = \sum_{i=1}^{r} \left(\frac{\sigma_i b_i}{\sigma_i^2 + \lambda}\mathbf{v}_i\right) \\
&\text{else} \\
&\qquad x = \sum_{i=1}^{r} \left(\frac{b_i}{\sigma_i}\right)\mathbf{v}_i \\
&\text{end}
\end{aligned}
$$

where $\mathbf{U}$ is $m \times m$ unitary matrix, $\mathbf{\Sigma}$ is $m \times n$ diagonal matrix with non-negative real diagonal elements $[\sigma_1, ..., \sigma_n]$ and $\mathbf{V}$ is $n \times n$ unitary matrix. Clearly, the computational complexity of Algorithm (A.12) contains the SVD computation and solving for λ. The algorithms used to compute the SVD are a combination of the Householder biadiagonalization algorithm and Golub-Kahan algorithm. On other hand, λ can be solved using Newton algorithm. Basically, the Problem (A.11) and Algorithm (A.12) is corresponding to CC element as described in previous section. As a result, the computation of SVD is needed only once for fixed CC scheme. However, in dynamic case the computation is done per spectral change. Consequently the

SVD computational complexity of $\mathbf{C}$ matrix is computed in the following way:

$$\begin{aligned}
\mathcal{C}_{SVD} =& \sum_{k=S-M+1}^{S} (k^3+k^2+2k+4) + \sum_{i=2}^{M-1}(i^3+i^2+2i+4) + \sum_{\substack{i=1 \\ k=S-M+1}}^{\substack{i=M \\ k=S}} k^2 i \\
&+ \sum_{\substack{i=2 \\ k=S-M+3}}^{\substack{i=M-1 \\ k=S}} ki^2 + Q\left[2M^4 - M^3 + 4M + 6 + S^3 + S^2M + SM^2\right] \\
\mathcal{A}_{SVD} =& \sum_{k=S-M+1}^{S} (k^3+2k^2+k+3) + \sum_{i=2}^{M-1}(i^3+2i^2+i+3) + \sum_{\substack{i=1 \\ k=S-M+1}}^{\substack{i=M \\ k=S}} k^2 i \\
&+ \sum_{\substack{i=2 \\ k=S-M+3}}^{\substack{i=M-1 \\ k=S}} ki^2 + Q\left[2M^4 - M^3 + 2M + 7 + S^3 + S^2M + SM^2\right] \\
\mathcal{D}_{SVD} =& \sum_{k=S-M+1}^{S} (k+2) + \sum_{i=2}^{M-1}(i+2) + Q[2M-2] \\
\mathcal{S}_{SVD} =& 2M - 2 + Q[2M-1]
\end{aligned} \tag{A.13}$$

where Q is the number of required iterations to evaluate the SVD components and $\mathcal{S}$ is the number of required square roots. Then, the computational complexity of dynamic unlimited CC can be calculated as follows:

$$\begin{aligned}
\mathcal{C} =& \mathcal{C}_{SVD} + S^2 + M^2 + 3M + L(6M+3) \\
\mathcal{A} =& \mathcal{A}_{SVD} + S^2 + 3M + L(6M+2) \\
\mathcal{D} =& \mathcal{D}_{SVD} + 2M + L(2M+1) \\
\mathcal{S} =& \mathcal{S}_{SVD}
\end{aligned} , \tag{A.14}$$

where L is the number of iterations required to solve for λ in Algorithm (A.12) using Newton algorithm. The resulting computational complexity in Equations (A.13) and (A.14) are based on the assumption of that $\mathbf{C}$ is full rank matrix. Hence, the computational complexity are the highest possible complexity. On other hand, computational complexity of fixed unlimited CC scheme can be evaluated using Equation (A.14) without considering the SVD computational complexity, which a dramatic computational complexity compared dynamic unlimited CC scheme.

A.2 Computational complexity of peaks evaluation block

In CC and SW technique, it is critical to get the values of either subcarrier or OFDM symbol values at the middle in between the subcarriers center. These values have to be as accurate as possible, since inaccurate values made the weight evaluation insignificant for sidelobe suppression. Hence, the effect of CP or windowing has to be considered, knowing that the peaks evaluation process is done before the IFFT block. The computational complexity of sidelobe points evaluation in Equation (3.9) is calculated as follows:

$$\begin{aligned} \mathcal{C} &= 2N_u S \\ \mathcal{A} &= 3N_u S \ . \\ \mathcal{D} &= N_u S \end{aligned} \tag{A.15}$$

Similarly, computing the $\mathbf{C}$ matrix is dependent on the Equation (3.10). Consequently, the computational complexity of $\mathbf{C}$ matrix can be calculated as follows:

$$\begin{aligned} \mathcal{C} &= 2MS \\ \mathcal{A} &= 3MS \ . \\ \mathcal{D} &= MS \end{aligned} \tag{A.16}$$

Computational complexity in Equation (A.16) can be skipped in fixed case since matrix $\mathbf{C}$ is calculated only once. Nevertheless, the computational complexity is changed to consider the windowing in the combination technique. Then the computational complexity is as follows:

$$\begin{aligned} \mathcal{C} &= 5N_u S \\ \mathcal{A} &= 4N_u S \ . \\ \mathcal{D} &= N_u S \end{aligned} \tag{A.17}$$

As a result, the computational complexity of the $\mathbf{C}$ matrix is computed in the following way:

$$\begin{aligned} \mathcal{C} &= 5MS \\ \mathcal{A} &= 4MS \ . \\ \mathcal{D} &= MS \end{aligned} \tag{A.18}$$

Similarly, the previous complexity is neglected in fixed CC schemes.